Spin Switching via Targeted Structural Distortion

Constantinos J. Milios,[†] Alina Vinslava,[‡] Wolfgang Wernsdorfer,[‡]
Alessandro Prescimone,[†] Peter A. Wood,[†] Simon Parsons,[†] Spyros P. Perlepes,[ǁ]
George Christou,[§] and Euan K. Brechin*,[†]

*Contribution from the School of Chemistry, The University of Edinburgh, West Mains Road,
Edinburgh, EH9 3JJ, UK, Laboratoire Louis Néel-CNRS, 38042 Grenoble, Cedex 9, France,
Department of Chemistry, University of Florida, Gainesville, Florida 32611-7200, and
Department of Chemistry, University of Patras, 26504 Patras, Greece*

Received January 26, 2007; E-mail: ebrechin@staffmail.ed.ac.uk

Abstract: The deliberate "stepwise" structural distortion of the $[Mn^{III}_6O_2(sao)_6(O_2CR)_2L_4]$ ($S = 4$, $U_{eff} = 28$ K) family of SMMs (where sao^{2-} is the dianion of salicylaldoxime or 2-hydroxybenzaldeyhyde oxime and L = MeOH, EtOH) *via* the use of derivatized oxime ligands and bulky carboxylates leads to a family of single-molecule magnets with larger spin ground states and enhanced blocking temperatures. Replacing sao^{2-} and HCO_2^- in the molecule $[Mn^{III}_6O_2(sao)_6(O_2CH)_2(MeOH)_4]$ (**1**), with $Et\text{-}sao^{2-}$ ($Et\text{-}saoH_2$ = 2-hydroxypropiophenone oxime) and $Me_3CCO_2^-$ (pivalate), produces the complex $[Mn^{III}_6O_2(Et\text{-}sao)_6(O_2CCMe_3)_2(EtOH)_5]$ (**2**) that displays an $S = 7$ ground state with $U_{eff} = 30$ K. Replacing $Me_3CCO_2^-$ with $PhCO_2^-$ produces the complex $[Mn^{III}_6O_2(Et\text{-}sao)_6(O_2CPh)_2(EtOH)_4(H_2O)_2]$ (**3**) that displays an $S = 12$ ground state with $U_{eff} = 53$ K. The ligand substitution invokes a subtle structural distortion to the core of the molecule evidenced by an increased "twisting" of the oxime moiety (Mn−N−O−Mn) and a change in carboxylate ligation, which, in turn, invokes a dramatic change in the observed magnetic properties by switching weak antiferromagnetic exchange to weak ferromagnetic exchange.

Introduction

When inorganic chemistry finally emerged as a distinct discipline in the 1950s, one of the driving forces was the application of physical methods to discover molecular structures and to determine the details of their electronic structures, so providing the basis for correlations between structure and properties. Among the methods that came into prominence at that time was the measurement of bulk magnetic susceptibility.[1] In the 1950s and 1960s it was Nyholm,[2] and Figgis and Lewis[3] who pioneered the field that became known as magnetochemistry. However, there is now a distinct field of study developing around the directed synthesis of new molecular compounds (often based on coordination complexes) that show varieties of magnetic behavior, the so named molecular magnetism.[4] Molecular magnetism designates a multidisciplinary field of research that focuses on the employment of molecular approaches to design, create, study, and use new classes of magnetic materials in which properties can be tuned at the molecular level. In the past two decades this field has rapidly evolved[5] from the design of new molecule-based magnets

possessing higher critical temperatures, toward the development of more complex magnetic materials with one or more functional properties of interest (bistable magnetic materials with switching properties or multifunctional materials coupling magnetism with a second property), to the synthesis and investigation of nanosized magnetic molecules and other nanostructures exhibiting quantum effects, and finally to materials processing aimed at application. An extensive class of nanosized magnetic molecules of great current interest are single-molecule magnets (SMMs).

SMMs[6] are molecular transition-metal clusters that can retain magnetization in the absence of a magnetic field below a blocking temperature without the need for long-range cooperative interaction. They represent the smallest possible magnetic storage device, which can potentially retain information in a single molecule rather than in a magnetic particle or array of particles. SMMs thus represent a molecular (or bottom-up approach) to nanoscale magnets and, thus, are significantly different from classical (or top-down) nanoscale magnets of metals, metal alloys, and metal oxides. These differences include crystallinity, solubility, monodispersity, and the existence of peripheral organic ligands that prevent communication between the magnetic cores of neighboring molecules and which can be varied using chemical methods. Such molecules straddle the

[†] The University of Edinburgh.
[‡] Laboratoire Louis Néel-CNRS.
[§] University of Florida.
[ǁ] University of Patras.

(1) Day P. *J. Chem. Soc., Dalton Trans.* **1997**, 701.
(2) Nyholm, R. S.; Tobe, M. L. *Adv. Inorg. Chem. Radiochem.* **1963**, *5*, 1.
(3) For example, see: Figgis, B. N.; Lewis, J. In *Modern Coordination Chemistry*; Lewis, J., Wilkins, R. G., Eds.; Interscience: New York, 1960; Chapter 6.
(4) Kahn, O. *Molecular Magnetism*; Wiley-VCH: New York, 1993.
(5) Coronado, E; Gatteschi, D. *J. Mater. Chem.* **2006**, *16*, 2515 (Editorial).
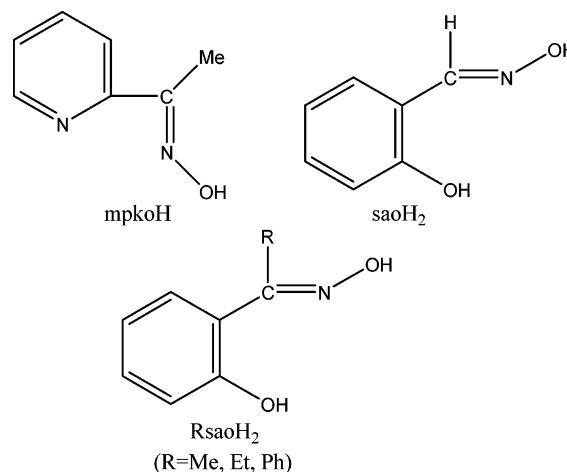
(6) For reviews, see: (a) Aromi, G.; Brechin, E. K. *Struct. Bonding* **2006**, *122*, 1. (b) Christou, G.; Gatteschi, D.; Hendrickson, D. N.; Sessoli, R. *MRS Bull.* **2000**, *25*, 66. (c) Gatteschi, D.; Sessoli, R. *Angew. Chem., Int. Ed.* **2003**, *42*, 268. (d) Bircher, R.; Chaboussant, G.; Dobe, C.; Güdel, H. U.; Ochsenbein, S. T.; Sieber, A.; Waldman, O. *Adv. Funct. Mater.* **2006**, *16*, 209.

classical/quantum interface in also displaying quantum tunneling of magnetization[7] and quantum phase interference.[8] The SMM behavior derives from the intrinsic intramolecular properties of a large spin ground state and a negative (easy-axis type) magnetoanisotropy.[6] As a result, SMMs possess a significant barrier to reversal (relaxation) of their magnetization vector, with the upper limit to this barrier (U) given by $S^2|D|$ and ($S^2 - {}^1/_4)|D|$ for integer and half-integer S values, respectively (S is the ground-state spin, and D, the axial zero-field splitting parameter). Experimentally, an SMM exhibits both a frequency-dependent, out-of phase alternating current (ac) magnetic susceptibility (χ_M'') signal and hysteresis loops in magnetization versus applied, direct current (dc) field studies.[6] SMMs have been proposed for several potential applications[9] including high-density information storage in which each bit of information is stored as the magnetization orientation of an individual molecule and as qubits for quantum computation where the required superposition of quantum states with opposite projections of spin are produced by quantum tunneling of the magnetization (QTM), intermolecular exchange, or multifrequency EPR pulses.

There are now several species displaying SMM behavior, the majority of which are transition metal clusters containing Mn ions, since Mn clusters often display large spin ground states and large and negative magnetoanisotropies associated with the presence of Jahn−Teller distorted Mn^{III} ions.[10] There is already one preparative route to new SMMs that starts from existing SMMs:[11] the modification of a given SMM structural type in a manner that does not change the core structure. Among other things, this allows researchers to tune the solubility, redox behavior, and magnetic properties of the molecules. It is important in this area of chemistry to not only make new examples of SMMs but also build up families of related compounds so that structure−property relations can be investigated.[12] For example, such studies on $[Mn_{12}O_{12}(O_2CR)_4(H_2O)_4]$ complexes have included variation of the carboxylate ligation,[13] variation of the oxidation level by cluster reduction,[14] and replacement of the carboxylate ligands with non-carboxylate groups.[15]

As part of our interest in the modification and reactivity properties of known SMMs, we have recently been turning our

(7) (a) Friedman, J. R.; Sarachik, M. P.; Tejada, J.; Ziolo, R. *Phys. Rev. Lett.* **1996**, *76*, 3830. (b) Thomas, L.; Lionti, F.; Ballou, R.; Gatteschi, D.; Sessoli, R.; Barbara, B. *Nature* **1996**, *383*, 145.
(8) Wernsdorfer, W.; Sessoli, R. *Science* **1999**, *284*, 133.
(9) Leuenberger, M. N.; Loss, D. *Nature* **2001**, *410*, 789. (b) Wernsdorfer, W.; Aliaga-Acalde, N.; Hendrickson, D. N.; Christou, G. *Nature* **2002**, *416*, 406. (c) Hill, S.; Edwards, R. S.; Aliaga-Acalde, N.; Christou, G. *Science* **2003**, *302*, 1015. (d) Tejada, J.; Chudnovsky, E. M.; del Barco, E.; Hernandez, J. M.; Spiller, T. P. *Nanotechnology* **2001**, *12*, 181.
(10) Cotton, F. A.; Wilkinson, G.; Murillo, C. A.; Bochmann, M. *Advanced Inorganic Chemistry*, 6th ed.; John Wiley and Sons: New York, 1999.
(11) (a) Christou, G. *Polyhedron* **2005**, *24*, 2065. (b) Chakov, N. E.; Zakharov, L. N.; Rheingold, A. L.; Abboud, K. A.; Christou, G. *Inorg. Chem.* **2005**, *44*, 4555.
(12) (a) Rajaraman, G.; Murugesu, M.; Sañudo, E. C.; Soler, M.; Wernsdorfer, W.; Helliwell, M.; Muryn, C.; Raftery, J.; Teat, S. J.; Brechin, E. K. *J. Am. Chem. Soc.* **2004**, *126*, 15445. (b) Brechin, E. K. *Chem. Commun.* **2005**, 5141.
(13) For example, see: Soler, M.; Artus, P.; Folting, K.; Huffman, J. C.; Hendrickson, D. N.; Christou, G. *Inorg. Chem.* **2001**, *40*, 4902.
(14) (a) Aubin, S. M. J.; Sun, Z.; Pardi, L.; Krzystek, J.; Folting, K.; Brunel, L.-C.; Rheingold, A. L.; Christou, G.; Hendrickson, D. N. *Inorg. Chem.* **1999**, *38*, 5329. (b) Soler, M.; Chandra, S. K.; Ruiz, D.; Huffman, J. C.; Hendrickson, D. N.; Christou, G. *Polyhedron* **2001**, *20*, 1279. (c) Chakov, N. E.; Soler, M.; Wernsdorfer, W.; Abboud, K. A.; Christou, G. *Inorg. Chem.* **2005**, *44*, 5304.
(15) (a) Artus, P.; Boscovic, C.; Yoo, J.; Streib, W. E.; Brunel, L.-C.; Hendrickson, D. N.; Christou, G. *Inorg. Chem.* **2001**, *40*, 4199. (b) Chakov, N. E.; Wernsdorfer, W.; Abboud, K. A.; Hendrickson, D. N.; Christou, G. *Dalton Trans.* **2003**, 2243.

Scheme 1. Structural Formulae of the Main Ligands Discussed in the Text

mpkoH

saoH$_2$

RsaoH$_2$
(R=Me, Et, Ph)

attention to the $[Mn^{III}_6O_2(sao)_6(O_2CR)_2L_4]$ family of SMMs,[16] where sao^{2-} is the dianion of salicylaldoxime or 2-hydroxy-benzaldeyhyde oxime (Scheme 1) and L is a coordinated solvent, normally alcohol. The core of these complexes contains a nonplanar $[Mn^{III}_6(\mu_3\text{-}O^{2-})_2(\mu_2\text{-}OR)_2]^{12+}$ unit of two off-set, stacked $[Mn^{III}_3(\mu_3\text{-}O^{2-})]^{7+}$ triangular subunits linked by two central oximato O atoms, with the remaining four sao^{2-} ligands bridging in an $\eta^1{:}\eta^1{:}\eta^1{:}\mu$ fashion along the edges of the $[Mn^{III}_3\text{-}(\mu_3\text{-}O^{2-})]^{7+}$ triangles. The four "central" metal ions are six-coordinate and in distorted octahedral geometries, while the outermost Mn ions have square pyramidal geometries with an axial contact of 3.5 Å to a phenolato oxygen. This paper first describes the preparation of a member of this family, namely the complex $[Mn_6O_2(sao)_2(O_2CH)_2(MeOH)_4]$ (**1**), using a microwave-assisted reaction. The complex displays an $S = 4$ spin ground state as a result of ferromagnetic exchange between the two antiferromagnetically coupled Mn^{III}_3 triangles. Taking complex **1** as a starting point, our goal was to prepare analogous complexes with sao^{2-}-based ligands derivatized at the oximate carbon atom *and* bulkier carboxylates. The initial stimulus came from the study of the origin of the ferromagnetic exchange in a recently reported[17] oxo-centered triangular Mn(III) SMM based on the derivatized oximate ligand methyl 2-pyridyl ketone oxime (mpkoH, Scheme 1); this ferromagnetic behavior is intriguing since the exchange in all other complexes containing the $[Mn^{III}_3(\mu_3\text{-}O^{2-})]^{7+}$ core, including the well-known "basic carboxylates" of general formula $[Mn^{III}_3O(O_2CR)_6L_3]^+$ (R = Me, Et, Ph; L = py, MeCN, H$_2$O, etc.),[18] is antiferromagnetic. We speculate that a structural distortion in the molecule caused primarily by the "*twisting*" of the oximato groups with regard to the Mn$_3$ plane is responsible. In order to evaluate the relative importance of this "*twisting*", we decided to use a family of ligands based on saoH$_2$ in which the oximate carbon atom has been derivatized to possess the "bulky" Me (MesaoH$_2$), Et (EtsaoH$_2$), and Ph (PhsaoH$_2$) groups (Scheme 1) in combination with "bulky" carboxylates and synthesized analogues of the

(16) Milios, C. J.; Raptopoulou, C. P.; Terzis, A.; Lloret, F.; Vicente, R.; Perlepes, S. P.; Escuer, A. *Angew. Chem., Int. Ed.* **2004**, *43*, 210.
(17) Stamatatos, Th. C.; Foguet-Albiol, D.; Stoumpos, C. C.; Raptopoulou, C. P.; Terzis, A.; Wernsdorfer, W.; Perlepes, S. P.; Christou, G. *J. Am. Chem. Soc.* **2005**, *127*, 15380.
(18) (a) Vincent, J. B.; Chang, H.-R.; Folting, K.; Huffman, J. C.; Christou, G.; Hendrickson, D. N. *J. Am. Chem. Soc.* **1987**, *109*, 5703. (b) Cannon, R. D.; White, R. P. *Prog. Inorg. Chem.* **1988**, *36*, 195.

Table 1. Crystallographic Data for Complexes **1**·4MeOH, **2**, and **3**·2EtOH

	1·4MeOH	2	3·2EtOH
formula[a]	$C_{52}H_{64}Mn_6N_6O_{26}$	$C_{74}H_{102}Mn_6N_6O_{23}$	$C_{80}H_{104}Mn_6N_6O_{26}$
fw	1518.67	1773.22	1895.30
cryst syst	triclinic	triclinic	triclinic
space group	$P\bar{1}$	$P\bar{1}$	$P\bar{1}$
T, K	150	150	150
λ, Å	Mo Kα (0.710 73 Å)	Mo Kα (0.710 73 Å)	Mo Kα (0.710 73 Å)
a, Å	9.3612(3)	13.486(3)	12.4947(9)
b, Å	12.8616(4)	14.882(3)	13.2846(9)
c, Å	13.8655(5)	20.822(4)	14.5047(11)
α, deg	107.441(2)	82.87(3)	71.488(4)
β, deg	96.022(2)	85.73(3)	82.305(4)
γ, deg	95.548(2)	76.51(3)	68.687(4)
V, Å^3	1569.4(1)	4027.6(15)	2126.4(3)
Z	1	2	1
ρ_{calcd}, g cm^{-3}	1.607	1.462	1.480(4)
μ (Mo, Kα), mm^{-1}	1.257	0.988	0.944
measd/indep (R_{int}) reflns	25 771/8856 (0.031)	47 310/19 012 (0.056)	49 242/11 741 (0.034)
obsd reflns [$I > 4\sigma(I)$]	6576	10875	8011
R1[b]	0.0363	0.0512	0.0339
wR2	0.1063	0.0282	0.1033
GOF on F^2	0.965	1.107	0.969
$\Delta\rho_{max,min}$, e Å^{-3}	0.72, −1.12	0.90, −0.74	0.55, −0.45

[a] $R_1 = \sum(|F_o| - |F_c|)/\sum(|F_o|)$. [b] $wR_2 = \{\sum[w(F_o^2 - F_c^2)^2]/\sum[w(F_o^2)^2]\}^{1/2}$.

SMM **1**. The central idea was to investigate whether the additional steric bulk would enforce similar minor structural distortions to that seen in the ferromagnetic $Mn_3/O^{2-}/mpko^-$ triangle[17] and the recently obtained ferromagnetic [Mn^{III}_4-(Mesao)$_4$(MesaoH)$_4$] "cube",[19] and thus switch the magnetic behavior from antiferromagnetic to ferromagnetic and improve the SMM properties. The present paper reports the realization of this idea; we show that it is indeed possible to *significantly* increase the ground state spin of **1** inducing a core perturbation (without core structural change) by controlled increase of the steric bulk within the oximate and carboxylate ligation. Specifically, we show that ligand-induced structural distortion of **1** with $S = 4$ causes the ground state to increase to $S = 7$ in [$Mn_6O_2(Etsao)_6(O_2CCMe_3)_2(EtOH)_5$] (**2**) and finally to $S = 12$ in the bulkiest derivative [$Mn_6O_2(Etsao)_6(O_2CPh)_2(EtOH)_4$-$(H_2O)_2$] (**3**). This increase in the ground state spin leads to enhanced SMM properties, with complex **3** displaying an effective energy barrier for magnetization reversal of ~53 K, double that observed for complex **1** and approaching the values observed for the prototype Mn_{12} SMMs. A preliminary communication of a part of this work has been published.[20]

Experimental Section

Materials and Physical Measurements. All manipulations were performed under aerobic conditions using materials as received (reagent grade). ***Caution***! Although we encountered no problems, care should be taken when using the potentially explosive perchlorate anion. 2′-Hydroxylpropiophenone oxime (EtsaoH$_2$, Scheme 1) was synthesized *via* the reaction of 2′-hydroxyropiophenone with hydroxylamine and sodium acetate in EtOH, as described in the literature.[21] Mn(O$_2$CPh)$_2$·2H$_2$O was prepared as previously decribed.[22] Elemental analyses (C, H, N) were performed by the EaStCHEM microanalysis service. IR
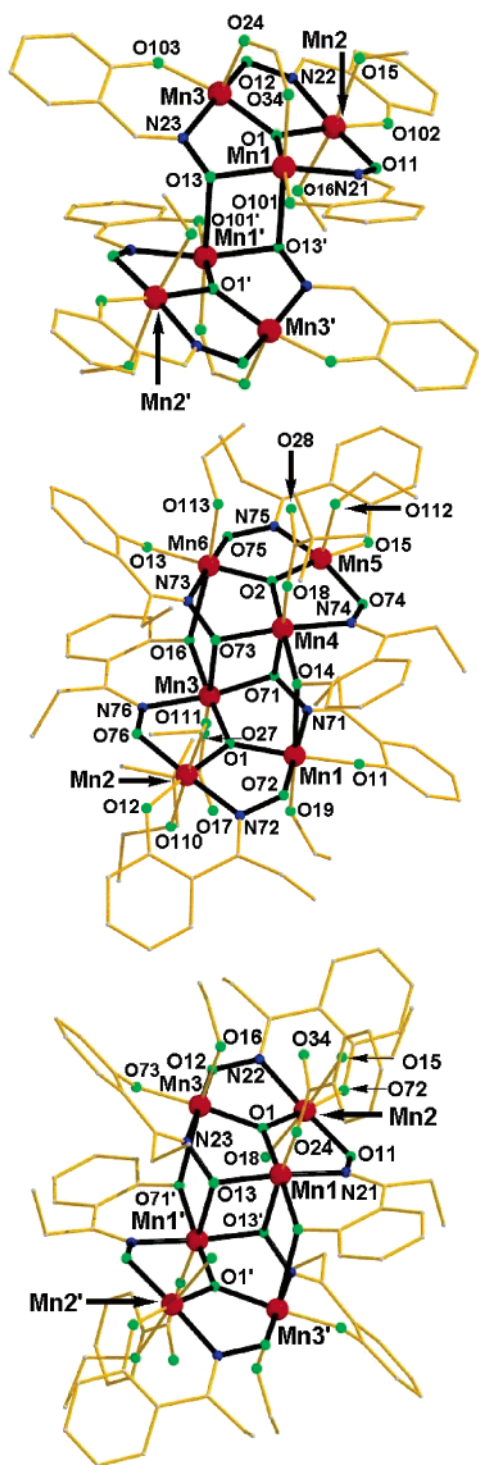
(19) Milios, C. J.; Prescimone, A.; Mishra, A.; Parsons, S.; Wernsdorfer, W.; Christou, G.; Perlepes, S. P.; Brechin, E. K. *Chem. Commun.* **2007**, *153*.
(20) (a) Milios, C. J.; Vinslava, A.; Whittaker, A. G.; Parsons, S.; Wernsdorfer, W.; Christou, G.; Perlepes, S. P.; Brechin, E. K. *Inorg. Chem.* **2006**, *45*, 5272. (b) Milios, C. J.; Vinslava, A.; Wood, P. A.; Parsons, S.; Wernsdorfer, W.; Christou, G.; Perlepes, S. P.; Brechin, E. K. *J. Am. Chem. Soc.* **2007**, *129*, 8.
(21) Dunsten, W. R.; Henry, T. A. *J. Chem. Soc.* **1899**, *75*, 66.
(22) Wemple, W. W.; Tsai, H.-L.; Wang, S.; Claude, J. P.; Streib, W.; Huffman, J. C.; Hendrickson, D. N.; Christou, G. *Inorg. Chem.* **1996**, *35*, 6437.

spectra were recorded as KBr pellets in the 4000−450 cm^{-1} range on a Jasco FT/IR-410 spectrometer. Variable-temperature, solid-state direct current (dc) magnetic susceptibility data down to 1.8 K were collected on a Quantum Design MPMS-XL SQUID magnetometer equipped with a 7 T dc magnet. Diamagnetic corrections were applied to the observed paramagnetic susceptibilities using Pascal's constants. Magnetic studies below 1.8 K were carried out on single crystals using a micro-SQUID apparatus operating down to 40 mK[23] and using a magnetometer consisting of a micro-Hall bar.

Preparation of the Complexes. [Mn$_6$O$_2$(sao)$_6$(O$_2$CH)$_2$(MeOH)$_4$]·4MeOH (1·4MeOH). Mn(ClO$_4$)$_2$·6H$_2$O (362 mg, 1.0 mmol), saoH$_2$ (137 mg, 1.0 mmol), NaOMe (108 mg, 2.0 mmol), and MeOH (8 mL) were placed in a sealed glass tube, which was then inserted into the cavity of a microwave reactor. The reaction mixture was maintained at $T = 110$ °C, power = 200 W, and pressure = 110 psi for a total of 5 min. After cooling (ca. 1 min), the solution was filtered and allowed to stand. Green-black crystals of **1**·4MeOH started to form immediately, and the reaction mixture was stored at room temperature for 24 h. The crystals were isolated by filtration, washed with a copious amount of Et$_2$O, and dried *in vacuo*; yield, ~80%. A sample for X-ray crystallography was kept in the mother liquor to prevent solvent loss. The dried sample was analyzed as lattice solvent-free (**1**). Anal. Calcd (found) for C$_{48}$H$_{48}$Mn$_6$N$_6$O$_{22}$: C, 41.45 (41.46); H, 3.49 (3.64); N, 6.04 (5.95). Main IR data (cm^{-1}, KBr pellet): 1597 (s), 1541 (s), 1471 (m), 1440 (s), 1282 (s), 1042 (s), 1028 (s), 919 (s), 753 (m), 680 (s), 652 (m), 475 (m).

[Mn$_6$O$_2$(Etsao)$_6$(O$_2$CCMe$_3$)$_2$(EtOH)$_5$] (2). MnCl$_2$·4H$_2$O (394 mg, 2.0 mmol), NaO$_2$CCMe$_3$ (620 mg, 5.0 mmol), EtsaoH$_2$ (330 mg, 2.0 mmol), and NEt$_3$ (0.5 mL) were stirred in EtOH (20 mL) for a period of 60 min. The solids soon dissolved, and the solution was then filtered and allowed to stand undisturbed at 20 °C for 3 days. Dark brown crystals of the product appeared, which were collected by filtration, washed with Et$_2$O (2 × 3 mL), and dried in air; yield, ~35%. Anal. Calcd (found) for C$_{74}$H$_{102}$Mn$_6$N$_6$O$_{23}$: C, 50.11 (50.19); H, 5.81 (5.67); N, 4.74 (4.78). Main IR data (cm^{-1}, KBr pellet): 1595 (s), 1567 (s), 1524 (s), 1480 (m), 1434 (s), 1313 (s), 1250 (m), 1231 (m), 1132 (m), 1071 (m), 1046 (s), 1004 (s), 941 (s), 852 (m), 753 (s), 683 (s), 572 (m), 481 (m).

[Mn$_6$O$_2$(Etsao)$_6$(O$_2$CPh)$_2$(EtOH)$_4$(H$_2$O)$_2$]·2EtOH (3·2EtOH). A stirred solution of Mn(O$_2$CPh)$_2$·2H$_2$O (660 mg, 2.0 mmol) in EtOH

(23) Wernsdorfer, W. *Adv. Chem. Phys.* **2001**, *118*, 99.

Figure 1. Molecular structures of complexes **1** (top), **2** (middle), and **3** (bottom). The cores are outlined in bold.

(20 mL) was treated with solid EtsaoH$_2$ (330 mg, 2.0 mmol) for a period of 50 min. The resulting deep green solution was filtered and allowed to stand undisturbed at 15 °C for 2 days. Dark brown crystals of **3·2EtOH** were precipitated, which were collected by filtration, washed with Et$_2$O (2 × 3 mL), and dried in vacuo; yield, ~45%. The dried sample was analyzed as lattice solvent-free (**3**). Anal. Calcd (found) for C$_{76}$H$_{92}$Mn$_6$N$_6$O$_{24}$: C, 50.61 (50.78); H, 5.15 (5.01); N, 4.66 (4.51). Main IR data (cm^{-1}, KBr pellet): 1594 (s), 1568 (s), 1524 (s), 1475 (m), 1435 (s), 1392 (s), 1312 (s), 1251 (m), 1232 (m), 1133 (m), 1095 (m), 1070 (m), 1046 (s), 1004 (s), 942 (s), 852 (m), 753 (m), 721 (m), 681 (s), 572 (m), 482 (m).

Table 2. Selected Interatomic Distances (Å) and Angles (deg) for **1·4MeOH**[a]

Mn(1)...Mn(2)	3.238(1)	Mn(2)−O(11)	1.918(2)
Mn(2)...Mn(3)	3.258(1)	Mn(2)−O(15)	2.245(2)
Mn(1)...Mn(3)	3.143(1)	Mn(2)−O(16)	2.262(2)
Mn(1)...Mn(1′)	3.337(1)	Mn(2)−O(102)	1.871(2)
Mn(1)−O(1)	1.872(2)	Mn(2)−N(22)	2.006(2)
Mn(1)−O(13)	1.948(2)	Mn(3)−O(1)	1.857(2)
Mn(1)−O(13′)	2.443(2)	Mn(3)−O(12)	1.898(2)
Mn(1)−O(34)	2.138(2)	Mn(3)−O(24)	2.112(2)
Mn(1)−O(101)	1.868(2)	Mn(3)−O(103)	1.862(2)
Mn(1)−N(21)	2.002(2)	Mn(3)−N(23)	1.997(2)
Mn(2)−O(1)	1.879(2)		
O(1)−Mn(1)−O(101)	176.1(1)	O(1)−Mn(3)−O(24)	95.1(1)
O(13)−Mn(1)−N(21)	165.3(1)	O(12)−Mn(3)−O(24)	99.0(1)
O(13′)−Mn(1)−O(34)	176.2(1)	O(24)−Mn(3)−O(103)	99.0(1)
O(1)−Mn(2)−O(102)	173.9(1)	O(24)−Mn(3)−N(23)	95.3(1)
O(11)−Mn(2)−N(22)	175.0(1)	Mn(1)−O(1)−Mn(2)	119.4(1)
O(15)−Mn(2)−O(16)	172.6(1)	Mn(2)−O(1)−Mn(3)	121.4(1)
O(1)−Mn(3)−O(103)	165.9(1)	Mn(1)−O(1)−Mn(3)	114.9(1)
O(12)−Mn(3)−N(23)	165.6(1)	Mn(1)−O(13)−Mn(1′)	98.3(1)

[a] Primed atoms are generated by the symmetry operation $-x, -y, -z + 1$.

Table 3. Selected Interatomic Distances (Å) and Angles (deg) for **2**

Mn(1)...Mn(2)	3.255(3)	Mn(3)−O(1)	1.876(3)
Mn(1)...Mn(3)	3.271(3)	Mn(3)−O(27)	2.104(3)
Mn(2)...Mn(3)	3.256(3)	Mn(3)−O(73)	2.517(3)
Mn(4)...Mn(5)	3.247(3)	Mn(4)−O(2)	1.883(3)
Mn(4)...Mn(6)	3.246(3)	Mn(4)−O(18)	2.131(3)
Mn(5)...Mn(6)	3.257(3)	Mn(4)−O(71)	2.390(3)
Mn(3)...Mn(4)	3.341(3)	Mn(5)−O(2)	1.864(3)
Mn(1)−O(1)	1.891(3)	Mn(5)−O(74)	1.911(3)
Mn(1)−O(14)	2.458(3)	Mn(5)−O(112)	2.135(3)
Mn(1)−O(19)	2.234(3)	Mn(6)−O(2)	1.892(3)
Mn(2)−O(1)	1.885(3)	Mn(6)−O(16)	2.388(3)
Mn(2)−O(110)	2.236(3)	Mn(6)−O(113)	2.212(3)
Mn(2)−O(111)	2.280(3)	Mn(6)−N(73)	1.988(3)
O(1)−Mn(1)−O(11)	176.4(1)	O(2)−Mn(5)−O(112)	92.0(1)
O(14)−Mn(1)−O(19)	169.1(1)	O(112)−Mn(5)−N(75)	100.8(1)
O(72)−Mn(1)−N(71)	175.8(1)	O(15)−Mn(5)−O(112)	95.3(1)
O(1)−Mn(2)−O(12)	176.9(1)	O(2)−Mn(6)−O(13)	175.3(1)
O(76)−Mn(2)−N(72)	175.9(1)	O(16)−Mn(6)−O(113)	164.8(1)
O(110)−Mn(2)−O(111)	177.7(1)	O(75)−Mn(6)−N(73)	174.4(1)
O(1)−Mn(3)−O(16)	168.7(1)	Mn(1)−O(1)−Mn(2)	119.1(1)
O(27)−Mn(3)−O(73)	171.0(1)	Mn(1)−O(1)−Mn(3)	120.6(1)
O(71)−Mn(3)−N(76)	166.7(1)	Mn(2)−O(1)−Mn(3)	119.9(1)
O(2)−Mn(4)−O(14)	168.0(1)	Mn(4)−O(2)−Mn(5)	120.2(1)
O(18)−Mn(4)−O(71)	177.7(1)	Mn(4)−O(2)−Mn(6)	118.6(1)
O(73)−Mn(4)−N(74)	172.5(1)	Mn(5)−O(2)−Mn(6)	120.3(1)
O(2)−Mn(5)−O(15)	172.7(1)	Mn(3)−O(71)−Mn(4)	100.3(1)
O(74)−Mn(5)−N(75)	161.4(1)	Mn(3)−O(73)−Mn(4)	96.1(1)

X-ray Crystallography and Structure Solution. Diffraction data were collected at 150 K on a Bruker Smart Apex CCDC diffractometer, equipped with an Oxford Cryosystems LT device, using Mo radiation. The structures were solved by direct methods (*SHELXS-86* for **1·4MeOH**, *SIR92* for **2**, *DIRDIF* for **3·2EtOH**) and refined by full-matrix least-squares techniques on F^2 (*CRYSTALS*).[24] Data collection parameters and structure solution and refinement details are listed in Table 1. Full details can be found in the CIF files provided in the Supporting Information.

Results and Discussion

Syntheses. The three complexes contain exclusively Mn^{III} ions (vide infra). Given that the starting Mn sources contain exclusively Mn^{II} ions, it is apparent that the Mn^{III} ions are

(24) Betteridge, P. W.; Carruthers, J. R.; Cooper, R. I.; Prout, K.; Watkin, D. J. *J. Appl. Crystallogr.* **2003**, *36*, 1487.

Table 4. Selected Interatomic Distances (Å) and Angles (deg) for 3·2EtOH[a]

Mn(1)...Mn(2)	3.258(1)	Mn(2)−O(11)	1.925(2)
Mn(2)...Mn(3)	3.237(1)	Mn(2)−O(15)	2.289(2)
Mn(1)...Mn(3)	3.280(1)	Mn(2)−O(18)	2.223(2)
Mn(1)...Mn(1′)	3.229(1)	Mn(2)−O(72)	1.885(2)
Mn(1)−O(1)	1.878(2)	Mn(2)−N(22)	2.006(2)
Mn(1)−O(13)	1.957(2)	Mn(3)−O(1)	1.888(2)
Mn(1)-O(13′)	2.423(2)	Mn(3)−O(12)	1.924(2)
Mn(1)−O(24)	2.118(2)	Mn(3)−O(16)	2.191(2)
Mn(1)−O(71)	1.908(2)	Mn(3)−O(71′)	2.488(2)
Mn(1)−N(21)	1.997(2)	Mn(3)−O(73)	1.867(2)
Mn(2)−O(1)	1.884(2)	Mn(3)−N(23)	2.000(2)
O(1)−Mn(1)−O(71)	169.5(1)	O(12)−Mn(3)−N(23)	179.4(1)
O(13)−Mn(1)−N(21)	172.1(1)	O(16)−Mn(3)−O(71′)	164.2(1)
O(13′)−Mn(1)−O(24)	172.6(1)	Mn(1)−O(1)−Mn(2)	120.0(1)
O(1)−Mn(2)−O(72)	175.9(1)	Mn(2)−O(1)−Mn(3)	118.2(1)
O(110)−Mn(2)−N(22)	175.9(1)	Mn(1)−O(1)−Mn(3)	121.1(1)
O(15)−Mn(2)−O(18)	174.8(1)	Mn(1)−O(13)−Mn(1′)	94.4(1)
O(1)−Mn(3)−O(73)	176.0(1)	Mn(1′)−O(71′)−Mn(3)	119.6(1)

[a] Primed atoms are generated by the symmetry operation $-x, -y, -z + 1$.

Table 5. Bond Valence Sum (BVS) Calculations[a] for Complexes 1·4MeOH, 2, and 3·2EtOH

	complex 1·4MeOH			complex 3·2EtOH		
	Mn^{II}	Mn^{III}	Mn^{IV}	Mn^{II}	Mn^{III}	Mn^{IV}
Mn(1)	3.38	*3.12*	3.06	3.31	*3.05*	2.97
Mn(2)	3.42	*3.16*	3.10	3.37	*3.10*	3.05
Mn(3)	3.39	*3.13*	3.07	3.33	*3.07*	3.01

	complex 2		
	Mn^{II}	Mn^{III}	Mn^{IV}
Mn(1)	3.36	*3.09*	3.04
Mn(2)	3.39	*3.13*	3.07
Mn(3)	3.30	*3.04*	2.99
Mn(4)	3.29	*3.03*	2.97
Mn(5)	3.33	*3.07*	3.01
Mn(6)	3.41	*3.14*	3.08

[a] The italicized value is the one closest to the charge for which it was calculated. The oxidation state of a particular atom can be taken as the nearest whole number to the italicized value.

Table 6. Mn−O−N−Mn Torsion Angles (deg) for Complexes 1·4MeOH, 2, and 3·2EtOH

|	complex 1·4MeOH	complex 3·2EtOH
Mn(2)−O(11)−N(21)−Mn(1)	25.6	31.3
Mn(1)−O(13)−N(23)−Mn(3)	18.0	39.9
Mn(3)−O(12)−N(22)−Mn(2)	10.4	38.2

	complex 2
Mn(1)−O(72)−N(72)−Mn(2)	36.9
Mn(3)−O(71)−N(71)−Mn(1)	42.1
Mn(2)−O(76)−N(76)−Mn(3)	23.3
Mn(5)−O(74)−N(74)−Mn(4)	32.4
Mn(4)−O(73)−N(73)−Mn(6)	42.2
Mn(6)−O(75)−N(75)−Mn(5)	16.7

generated upon oxidation by atmospheric O_2, a process very common in Mn cluster chemistry, even in reducing solvents. The presence of the dianionic form of the oxime ligand (sao^{2-}, Etsao^{2-}) in the three complexes is a consequence of the 2:1, 2.5:1, and 2:1 MeO$^-$/saoH$_2$ (complex **1**), Me$_3$CCO$_2^-$/EtsaoH$_2$ (complex **2**) and PhCO$_2^-$/EtsaoH$_2$ (complex **3**) ratios, respectively, used in the reactions.

Complex **1** was initially isolated from the microwave-assisted reaction of Mn(ClO$_4$)$_2$·6H$_2$O with saoH$_2$ in the presence of

Scheme 2. Crystallographically Established Coordination Modes of the Ligands sao^{2-} and Etsao^{2-} in Complexes **1**−**3**
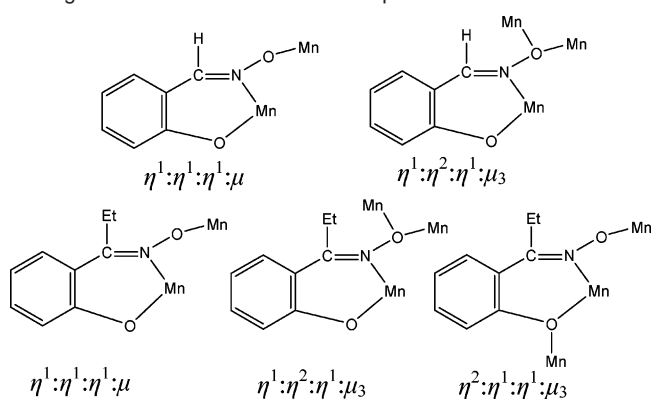
NaOMe in MeOH; the total reaction time was 5 min. The complex formed immediately upon cooling, and after 24 h the yield was approximately 80%. In the first experiments the sample was heated for 10 min, but we later found that reducing the reaction time to 5 min had no adverse effects on the yield of the product. A point of synthetic interest that deserves a comment is the presence of formate ligands in the product. The formate ions were derived from the (high-temperature/pressure-assisted) oxidation of the solvent or/and MeO$^-$ which is probably facilitated by the oxidizing character of Mn^{III}. There is precedent for similar MeOH or MeO$^- \rightarrow$ HCO$_2^-$ transformations in 3d-metal cluster chemistry.[25]

Recent work from our group[20a,26] has demonstrated that the use of microwave heating is a new and appealing approach for the synthesis of large polymetallic transition-metal cluster compounds. Compared to conventional methods of heating, it may lead to novel products by permitting access to alternative kinetic pathways, stabilizing different energy minima in a particular reaction system. It has also provided a means of improving the yields and reproducibility of known clusters (in general, these problems become more serious as the nuclearity of the product increases) in shorter reaction times and indeed may even be considered a *green* approach to the synthesis of metal clusters, since it employs minimal solvent and minimizes energy and heat loss *via* the *direct* heating of the sample. Compound **1** can be prepared by repeating the reaction under ambient conditions, i.e., without microwave irradiation, but crystalline material does not appear immediately; indeed, the maximum yield of ~30% is only achieved after a 60-min reaction and a 5-day crystallization period. The same complex can also be isolated from the Mn(O$_2$CH)$_2$·xH$_2$O/saoH$_2$/NaOMe reaction mixture in MeOH, i.e., replacing Mn(ClO$_4$)$_2$·6H$_2$O with Mn(O$_2$CH)$_2$·xH$_2$O in an otherwise identical reaction. Alternatively, **1** can be made by replacing NaOMe with NBu$^n_4$MnO$_4$. The procedure involves a comproportionation reaction between Mn(O$_2$CH)$_2$·xH$_2$O and NBu$^n_4$MnO$_4$ in a ~3:1 ratio in the presence of saoH$_2$ in MeOH. Comproportionation reactions between Mn^{II} and Mn^{VII} sources have found extensive use in

(25) (a) Biswas, B.; Khanra, S.; Weyhermüller, T.; Chaudhuri, P. *Chem. Commun.* **2007**, 1059. (b) Norman, R. E.; Leising, R. A.; Yan, S.; Que, L., Jr. *Inorg. Chim. Acta* **1998**, *273*, 393.
(26) Gass, I. A.; Milios, C. J.; Whittaker, A. G.; Fabiani, F. P. A.; Parsons S.; Murrie, M.; Perlepes, S. P.; Brechin, E. K. *Inorg. Chem.* **2006**, *45*, 5281. (b) Milios, C. J.; Prescimone, A.; Sanchez-Benitez, J.; Parsons, S.; Murrie, M.; Brechin, E. K. *Inorg. Chem.* **2006**, *45*, 7053. (c) Milios, C. J.; Whittaker, A. G.; Brechin, E. K. *Polyhedron* **2006**, DOI:10.1016/j.poly.2006.09.072.
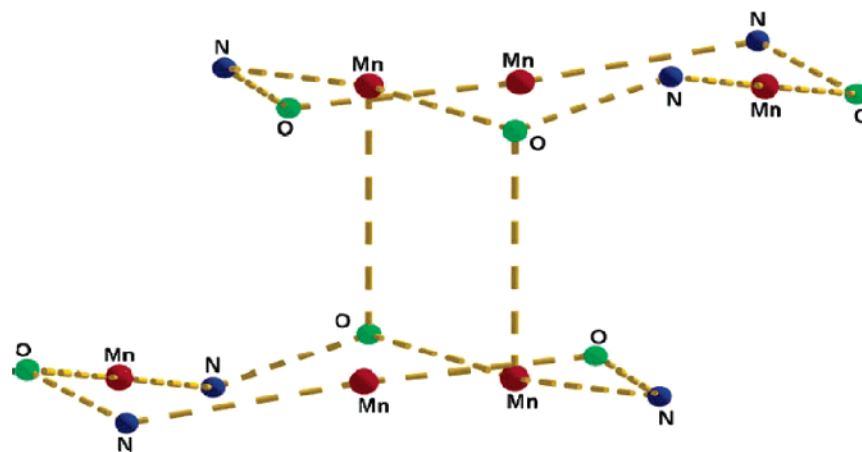
Figure 2. "*Twisted*" Mn−O−N−Mn arrangement of the Etsao^{2-} ligands in complex **3**.
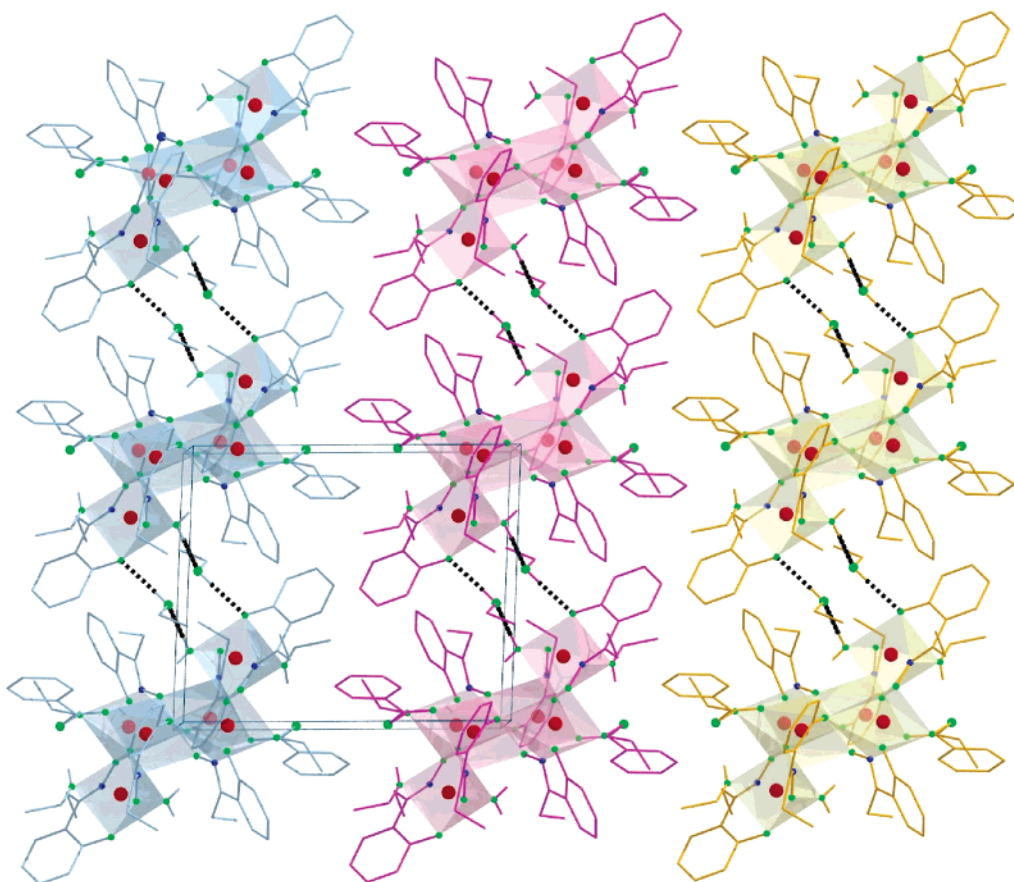
Figure 3. Packing of **3** in the crystal, highlighting the H-bonded 1D "zigzag" chains. Molecules of the same color belong to the same H-bonded channel.
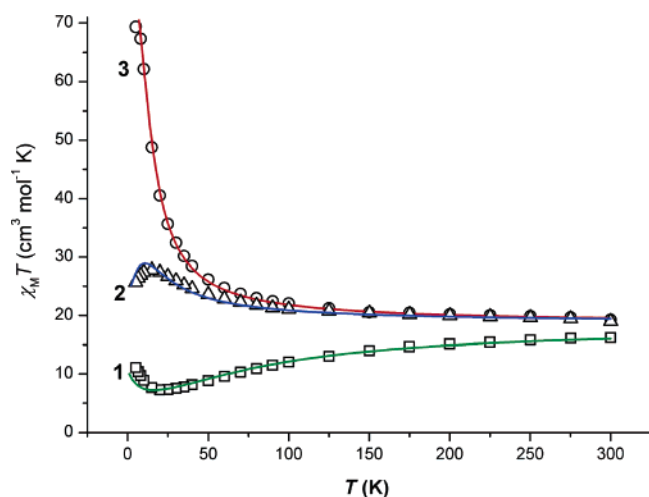
the production of higher oxidation state Mn carboxylate clusters of various nuclearities.[22,27]

Complex **1** has an $S = 4$ ground state and displays SMM behavior (vide infra). In an attempt to increase the ground state spin and improve the SMM properties of this complex by introducing steric bulk within the oximate and carboxylate ligation, we sought the Me$_3$CCO$_2^-$/Etsao^{2-} analogue of **1**. The 1:2.5:1 MnCl$_2$·4H$_2$O/NaO$_2$CCMe$_3$/EtsaoH$_2$ reaction mixture in EtOH, in the presence of a small, nonstoichiometric quantity

(27) (a) Milios, C. J.; Kyritsis, P.; Raptopoulou, C. P.; Terzis, A.; Vicente, R.; Escuer, A.; Perlepes, S. P. *Dalton Trans.* **2005**, *501*. (b) Harden, N. C.; Bolcar, M. A.; Wernsdorfer, W.; Abboud, K. A.; Streib, W. E.; Christou, G. *Inorg. Chem.* **2003**, *42*, 7067.

of NEt$_3$, yielded the desired complex [Mn$_6$O$_2$(Etsao)$_6$(piv)$_2$-(EtOH)$_5$] (**2**) in moderate yield. The role of NEt$_3$ is dual: it helps the double deprotonation of the oxime ligand, as well as the rapid oxidation of the Mn^{II} starting material. The same product can also be isolated in the absence of base, but longer periods of stirring are required in order for Mn^{II} to be oxidized to Mn^{III}, as is evidenced from the color of the reaction solution which darkens slowly upon stirring. Complex **2** displays an $S = 7$ ground state.
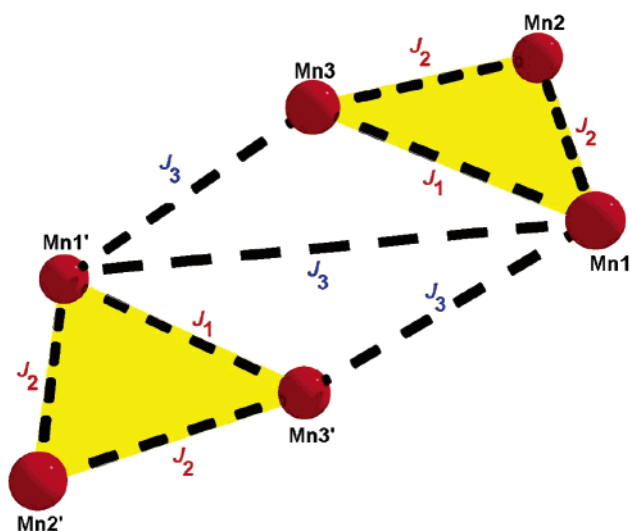
Our next goal was to investigate whether additional steric bulk on the carboxylate would enforce further structural distortions of the core, switch the magnetic behavior from

Figure 4. Plot of $\chi_M T$ *vs* T for complexes **1**−**3**. The solid lines represent simulations of the experimental data in the temperature range 300−5 K; see text for details.

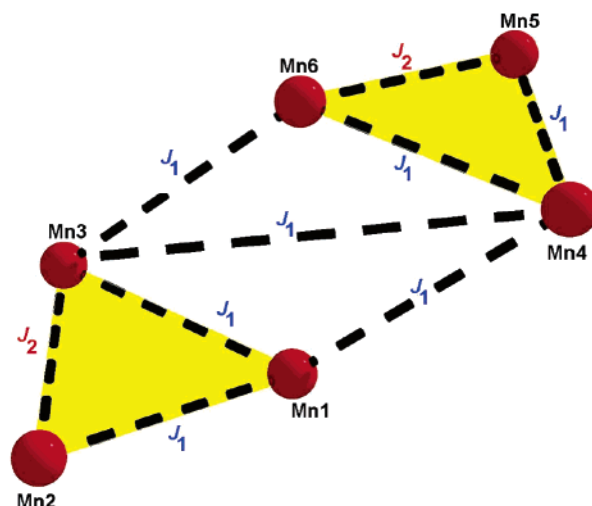**Scheme 3.** Exchange Interaction Model Used for Complex **1**; See Text for Details

Scheme 4. Exchange Interaction Model Used for Complex **2**; See Text for Details

Scheme 5. Exchange Interaction Model Used for Complex **3**; See Text for Details

antiferromagnetic/ferromagnetic to ferromagnetic, and significantly improve the SMM properties. The complex which fulfilled our plans was $[Mn_6O_2(Etsao)_6(O_2CPh)_2(EtOH)_4(H_2O)_2]$ (**3**) made *via* the 1:1 $Mn(O_2CPh)_2 \cdot 2H_2O/EtsaoH_2$ reaction mixture. This gave a deep green solution from which deposited the desired dark brown product on standing at room temperature.
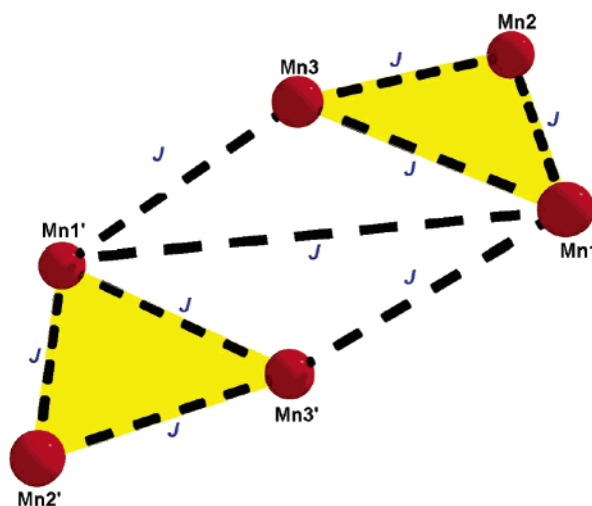
Two bands, one strong at ∼1595 cm^{-1} and one of medium intensity at ∼1250 cm^{-1}, are common in the IR spectra of **1**−**3**. These bands are assigned to the oximate $\nu(C=N)$ and $\nu(N-O)$ vibrational modes,[28] respectively, although the higher-wavenumber band may also have aromatic and/or carboxylate character. The spectra of the three complexes exhibit a strong and sharp band at ∼680 cm^{-1} assigned[18b] to the $\nu_{as}(Mn^{III}{}_3O)$ mode.

Description of Structures. The molecular structures of complexes **1**, **2**, and **3** are presented in Figure 1. Selected interatomic distances and angles are listed in Tables 2−4. Bond

valence sum (BVS) calculations for the metal ions of the three complexes are given in Table 5, while all the Mn−O−N−Mn torsion angles are listed in Table 6. For the sake of brevity, references to specific atoms in the following discussion for **1** and **3** implicitly include their symmetry-related partners. All the Mn atoms in the three molecules are in the 3+ oxidation state. The oxidation states of the metal ions were assigned using a combination of charge-balance and bond-length considerations and BVS calculations.[29] The six-coordinate Mn^{III} centers exhibit a Jahn−Teller (JT) distortion, as expected for a high-spin d^4 ion in near-octahedral geometry. As is almost always the case for Mn^{III} ions, the JT distortion is an axial elongation. Normally, JT elongation axes avoid Mn^{III}−O^{2-} bonds,[30] almost always the strongest and shortest in the molecules; complexes **1**−**3** are no exceptions.

Complex **1**·4MeOH crystallizes in the triclinic space group $P\bar{1}$, with the molecule lying on an inversion center. The

(28) (a) Chaudhuri, P.; Birkelbach, F.; Winter, M.; Staemmler, V.; Fleischhauer, P.; Haase, W.; Flörke, U.; Haupt, H.-J. *J. Chem. Soc., Dalton Trans.* **1994**, 2313. (b) Chaudhuri, P.; Rentschler, E.; Birkelbach, F.; Krebs, C.; Bill, E.; Weyhermüller, T.; Flörke, U. *Eur. J. Inorg. Chem.* **2003**, 541.

(29) (a) Thorp, H. H. *Inorg. Chem.* **1992**, *31*, 1585. (b) Liu, W.; Thorp, H. H. *Inorg. Chem.* **1993**, *32*, 4102. (c) Palenik, G. J. *Inorg. Chem.* **1997**, *36*, 4888.
(30) Chakov, N. E.; Lee, S.-C.; Harter, A. G.; Kuhns, P. L.; Reyes, A. P.; Hill, S. O.; Dalal, N. S.; Wernsdorfer, W.; Abboud, K. A.; Christou, G. *J. Am. Chem. Soc.* **2006**, *128*, 6975.
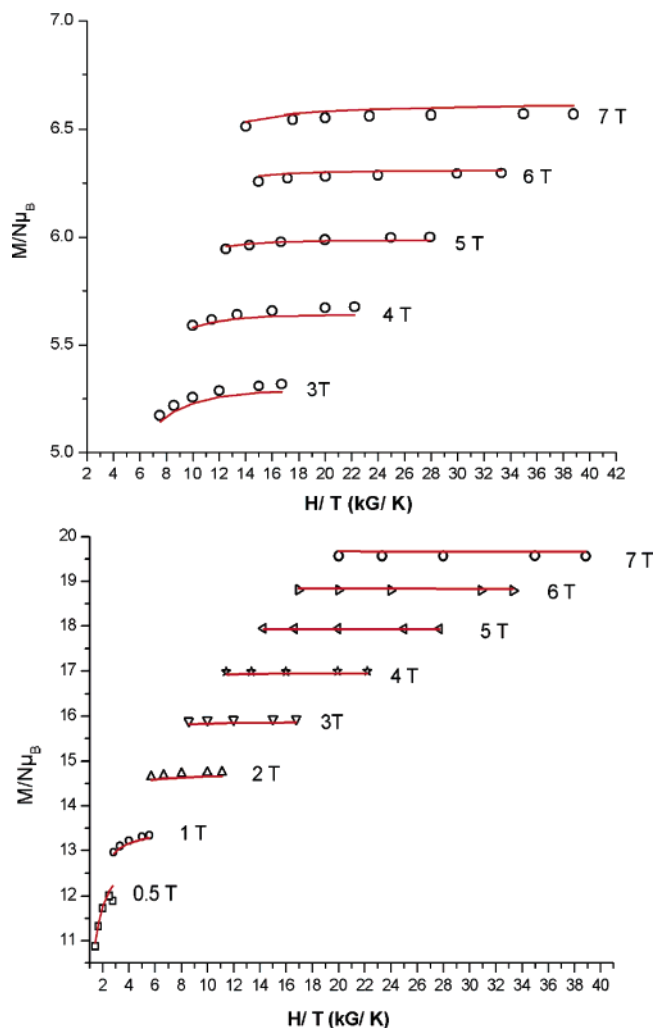
Figure 5. Plot of reduced magnetization ($M/N\mu_B$) versus H/T for **1** (top) and **3** (bottom). The solid lines correspond to the fits of the data; see text for details.

molecule contains the $[Mn^{III}_6(\mu_3\text{-}O)_2(\mu\text{-}OR)_2]^{12+}$ core, whose topology consists of six Mn^{III} ions arranged as two centrosymmetrically related off-set, stacked $[Mn^{III}_3(\mu_3\text{-}O)_2]^{7+}$ triangular subunits linked at one of their apexes [Mn(1), Mn(1′)] by two oximate O atoms [O(13)]. Considering the oximate N atoms as part of the core, this can be described as $[Mn^{III}_6(\mu_3\text{-}O)_2(\mu_3\text{-}ONR)_2(\mu\text{-}ONR)_4]^{8+}$. Two Mn_2 edges [Mn(1)...Mn(2), Mn-(2)...Mn(3)] are each bridged by one diatomic oximate group from one $\eta^1:\eta^1:\eta^1:\mu$ sao^{2-} ligand (Scheme 2). The remaining edge [Mn(1)...Mn(3)] is bridged by the diatomic oximate group from an $\eta^1:\eta^2:\eta^1:\mu_3$ sao^{2-} ligand (Scheme 2) and an $\eta^1:\eta^1:\mu$ formate ligand. Two terminal MeOH molecules complete the coordinate sphere of Mn(2). The Mn(1)...Mn(3) separation [3.143(1) Å] is shorter than the other two [3.238(1), 3.258(1) Å], presumably due to the presence of the extra formate bridge; the triangle is thus approximately isosceles. Ions Mn(1) and Mn-(2) are bound to an O_5N set of donor atoms and display JT elongation; the JT axes are O(13′)−Mn(1)−O(34) and O(15)−Mn(2)−O(16). Mn(3) is five-coordinate (the donor set is O_4N) and has a distorted square-pyramidal geometry, with the formate oxygen O(24) at the apical position. The Mn(3)...O(101′) distance is 3.524(2) Å. The four JT axes and the apical bonds of the five-coordinate Mn^{III} ions are approximately co-parallel, all perpendicular to the Mn_3 planes. Using the perspective view

of Figure 1, the central $\mu_3\text{-}O^{2-}$ ion O(1′) in one triangular unit is *above* (0.23 Å) the Mn_3 plane that it bridges [Mn(1′)Mn(2′)-Mn(3′)], while its symmetry-related partner O(1) is 0.23 Å *below* the Mn(1)Mn(2)Mn(3) plane; i.e., the two oxide ligands are directed toward the inside of the hexanuclear core. Four of the sao^{2-} ligands adopt the common $\eta^1:\eta^1:\eta^1:\mu$ coordination mode (Scheme 2), while the other two adopt the rare $\eta^1:\eta^2:\eta^1:\mu_3$ mode (Scheme 2). The $\eta^1:\eta^2:\eta^1:\mu_3$ ligation mode has been observed in the structurally similar $[Mn_6O_2(sao)_6(O_2CR)_2(EtOH)_4]$ complexes (R = Me, Ph),[16] in the $[M^{III}_6O_2(sao)_6(O_2CR)_2(OH_2)_2\text{-}(R'CN)_2]$ (M = V, Cr, Fe; RCO$_2^-$ = Ph$_3$CCO$_2^-$, Me$_3$CCO$_2^-$, Ph$_2$C(OH)CO$_2^-$, PhCO$_2^-$, EtCO$_2^-$) family of clusters,[31] in $[Fe_6O_2(O_2CPh)_{10}(sao)_2L_2]$ (L = MeCONH$_2$, H$_2$O),[32] and also in trinuclear and tetranuclear complexes.[33] In the crystal lattice there are a number of significant intermolecular interactions: each [Mn$_6$] molecule forms eight H-bonds to the four MeOH solvate molecules: two involving two terminal MeOH molecules, four involving four phenolato oxygen atoms, and two involving two oximato oxygens. The closest intermolecular Mn···Mn distance is 6.539(2) Å.

Compound **1** is the fourth structurally characterized *homometallic* Mn complex with the mono- (saoH$^-$) or/and the dianion (sao^{2-}) of 2-hydroxybenzaldeyhde as ligand. The other three complexes are the above-mentioned, structurally similar $[Mn_6O_2(sao)_6(O_2CR)_2(EtOH)_4]$ complexes (R = Me, Ph),[16] and the butterfly-type cluster $[Mn^{III}_4O_2(sao)_2(dpg)_3L_2](ClO_4)$,[28b] where dpg is the diphenylglycolate ligand and L is the capping ligand 1,4,7-trimethyl-1,4,7-triazacyclononane. However, *heterometallic* Mn$^{III}_2$Fe$^{III}_2$/sao^{2-} clusters have been reported.[28]

Complex **2** also crystallizes in the triclinic space group $P\bar{1}$, and its molecular structure (Figure 1) is analogous to that of **1**·4MeOH, despite the lack of an inversion center in the molecule of the former (*C*1 symmetry). Ions Mn(3) and Mn(4) in the structure of **2** "correspond" to ion Mn(1) in the structure of **1**·4MeOH, and ions Mn(2) and Mn(5) of **2**, to ion Mn(2) of **1**·4MeOH, while ions Mn(1) and Mn(6) of **2** have a clear analogy with ion Mn(3) of **1**·4MeOH. However, the increased steric bulk of the Me$_3$CCO$_2^-$ and Etsao^{2-} ligands causes a shortening of the phenolato oxygen atoms [O(14) and O(16)] distances to Mn(1) and Mn(6), respectively, and thus the Mn-(1)...O(14) [2.458(3) Å] and Mn(6)...O(16) [2.388(3) Å] distances can be considered as representing weakly bonding interactions. Note that "these" metal ions were truly five-coordinate in **1**. The increased steric bulk also causes a severe twisting of the Mn−O−N−Mn moieties within each Mn$_3$ subunit; this is evidenced by the average Mn−O−N−Mn torsion angle, which in **1** is $\alpha_v = 18.0°$ compared to $\alpha_v = 34.1°$ [for the Mn(1)Mn(2)Mn(3) subunit] and 30.4° [for the Mn(4)Mn-(5)Mn(6) subunit] in **2** (see Table 6). This structural feature will be of relevance to the magnetic discussion later (vide infra). This also results in a change in the coordination of the carboxylates: from $\eta^1:\eta^1:\mu$ in **1** to the monodentate terminal (η^1) in the Me$_3$CCO$_2^-$/Etsao^{2-} cluster **2**, with the "vacant" site

(31) Chaudhuri, P. *Coord. Chem. Rev.* **2003**, *243*, 143.
(32) Raptopoulou, C. P.; Boudalis, A. K.; Sanakis, Y.; Psycharis, V.; Clemente-Juan, J. M.; Fardis, M.; Diamantopoulos, G.; Papavassiliou, G. *Inorg. Chem.* **2006**, *45*, 2317.
(33) (a) Thorpe, J. M.; Beddoes, R. L.; Collison, D.; Garner, C. D.; Helliwell, M.; Tasker, P. A. *Angew. Chem. Int. Ed.* **1999**, *38*, 1119. (b) Chaudhuri, P.; Hess, M.; Rentschler, E.; Weyhermüller, T.; Flörke, U. *New J. Chem.* **1998**, 553. (c) Zerbib, V.; Robert, F.; Gouzerh, G. *J. Chem. Soc., Chem. Commun* **1994**, 2179. (d) Smith, A. G.; Tasker, P. A.; White, D. J. *Coord. Chem. Rev.* **2003**, *241*, 61.
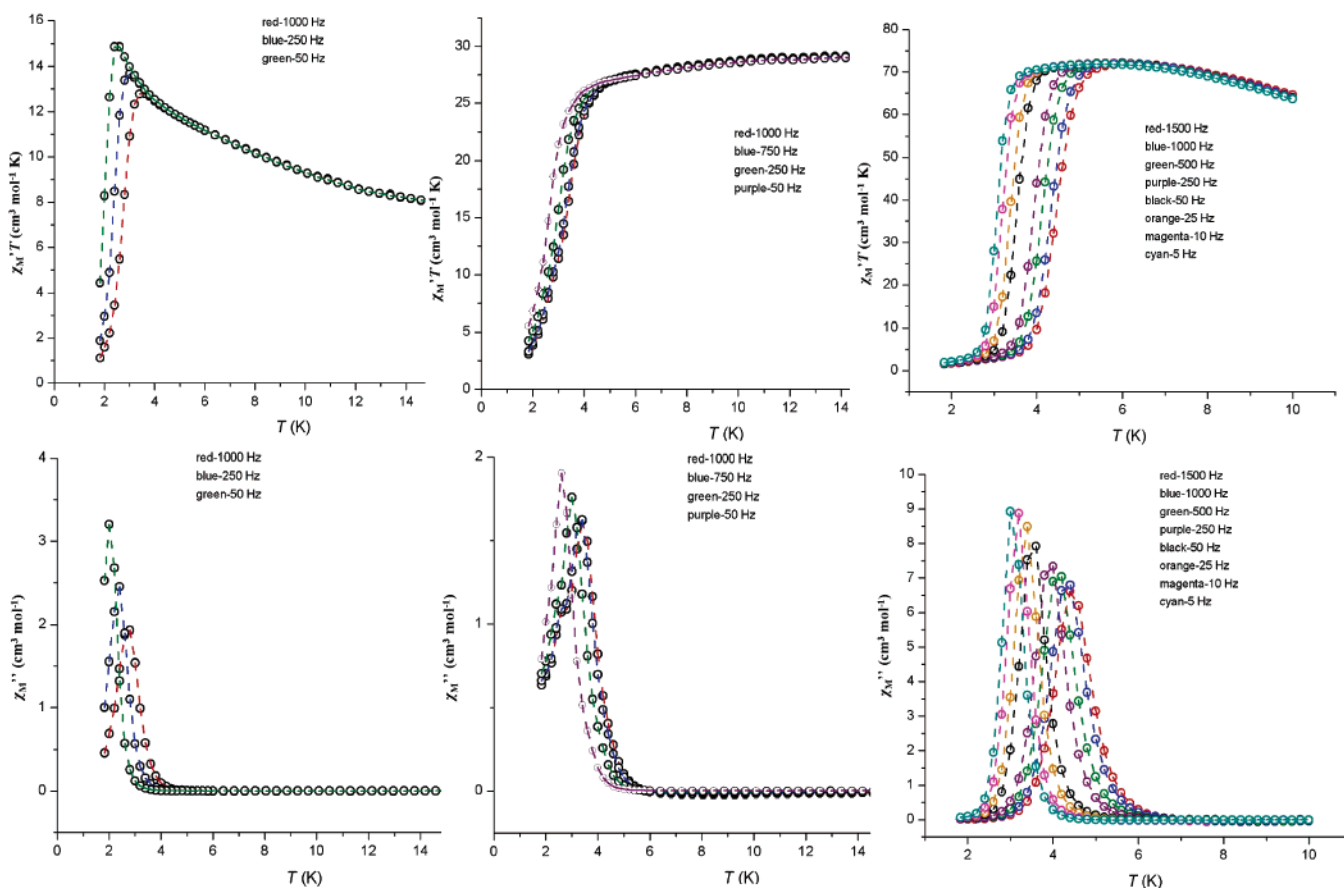
Figure 6. Plots of the in-phase $\chi_M'T$ (top) and out-of-phase χ_M'' (bottom) ac susceptibility measurements for **1**–**3** (left to right) at the indicated temperature and frequency ranges.

on Mn(1) and Mn(6) now occupied by an additional solvent (EtOH) molecule. The absence of carboxylate bridging makes the Mn(1)Mn(2)Mn(3) and Mn(4)Mn(5)Mn(6) triangles approximately equilateral (Table 3). However, the molecule of **2** has only one coordinated alcohol molecule more than **1** (5 vs 4), because ion Mn(5) in the former is clearly five-coordinate and lacks the second EtOH ligand. Mn(2) has a distorted square-pyramidal geometry, with the EtOH oxygen O(112) at the apical position.

Ions Mn(1), Mn(2), Mn(3), Mn(4), and Mn(6) are bound to an O_5N set of donor atoms. The JT axes are O(14)−Mn(1)−O(19), O(110)−Mn(2)−O(111), O(27)−Mn(3)−O(73), O(18)−Mn(4)−O(71), and O(16)−Mn(6)−O(113). The five JT axes and the apical bond of Mn(5) are approximately coparallel. Since the Mn(3)−O(73) distance is long [2.517(3) Å], this metal ion can be described as "pseudo" six-coordinate or even five-coordinate. The dihedral angle between the Mn(1)Mn(2)Mn(3) and Mn(4)Mn(5)Mn(6) planes is only 3.5°. Using the perspective view of Figure 1, the μ_3-O^{2-} ion O(1) is slightly *below* (0.071 Å) the Mn_3 plane that it bridges [Mn(1)Mn(2)Mn(3)], while the μ_3-O^{2-} ion O(2) of the other triangular subunit is 0.105 Å *above* the Mn(4)Mn(5)Mn(6) plane; i.e., the two oxide ligands are directed toward the outside of the hexanuclear core. In the crystal the clusters have little intermolecular contact; there are no H-bonds present, and the closest Mn···Mn distance is 9.646 Å.

It is somewhat surprising to witness the variety of coordination modes adopted by the doubly deprotonated Etsao^{2-} ligand in just one molecule: three distinct coordination modes that

bridge up to three metal ions, proving the great versatility (and hence potential) of this and similar ligands in transition-metal cluster chemistry. Two Etsao^{2-} ligands adopt the η^1:η^1:η^1:μ mode and two adopt the η^1:η^2:η^1:μ_3 mode, while the remaining Etsao^{2-} ions are in the novel (for this saoH$_2$-based family of ligands) η^2:η^1:η^1:μ_3 ligation mode. These modes are illustrated in Scheme 2. Thus the core of the complex appears to be [Mn$^{III}_6$-(μ_3-O)$_2$(μ-OR)$_2$(μ-OR′)$_2$]$^{10+}$; a more detailed description of the core is [Mn$^{III}_6$(μ_3-O)$_2$(μ_3-ONR)$_2$(μ-ONR)$_4$(μ-OR′)$_2$]$^{6+}$.

Complex **3**·2EtOH crystallizes in the triclinic space group $P\bar{1}$, with the molecule lying on an inversion center. Its molecular structure is analogous to that of **2**. However, the structural modification of the core is now more pronounced compared to that in **2**. Again there is a severe twisting of the Mn−O−N−Mn moieties (i.e., the oximate linkages) within each Mn$_3$ subunit (Figure 2), and the carboxylate group is monodentate. The average Mn−O−N−Mn torsion angle in **3** is $\alpha_v = 36.5°$ (Table 6); the corresponding values for **1** and **2** are 18.0° and 34.1°/30.4°, respectively. The result of this significant distortion is a switch in one intratriangular magnetic exchange interaction from antiferromagnetic in **2** to ferromagnetic in **3** and thus the stabilization of an $S = 12$ ground state in the latter (vide infra).

The donor atom sets in the molecule of **3** are (μ_3-O^{2-})-(μ-$O_{oximate}$)$_2$(μ-$O_{phenolate}$)($O_{benzoate}$)N for Mn(1), (μ_3-O^{2-})($O_{oximate}$)-($O_{phenolate}$)(O_{aquo})($O_{ethanol}$)N for Mn(2), and (μ_3-O^{2-})($O_{oximate}$)-(μ-$O_{phenolate}$)($O_{phenolate}$)($O_{ethanol}$)N for Mn(3). The parallel JT axes are O(13′)−Mn(1)−O(24), O(15)−Mn(2)−O(18), and O(16)−Mn(3)−O(71′). If one considers the Mn(1)−O(13′) [2.423(2) Å] and Mn(3)−O(71′) [2.488(2) Å] distances too long for
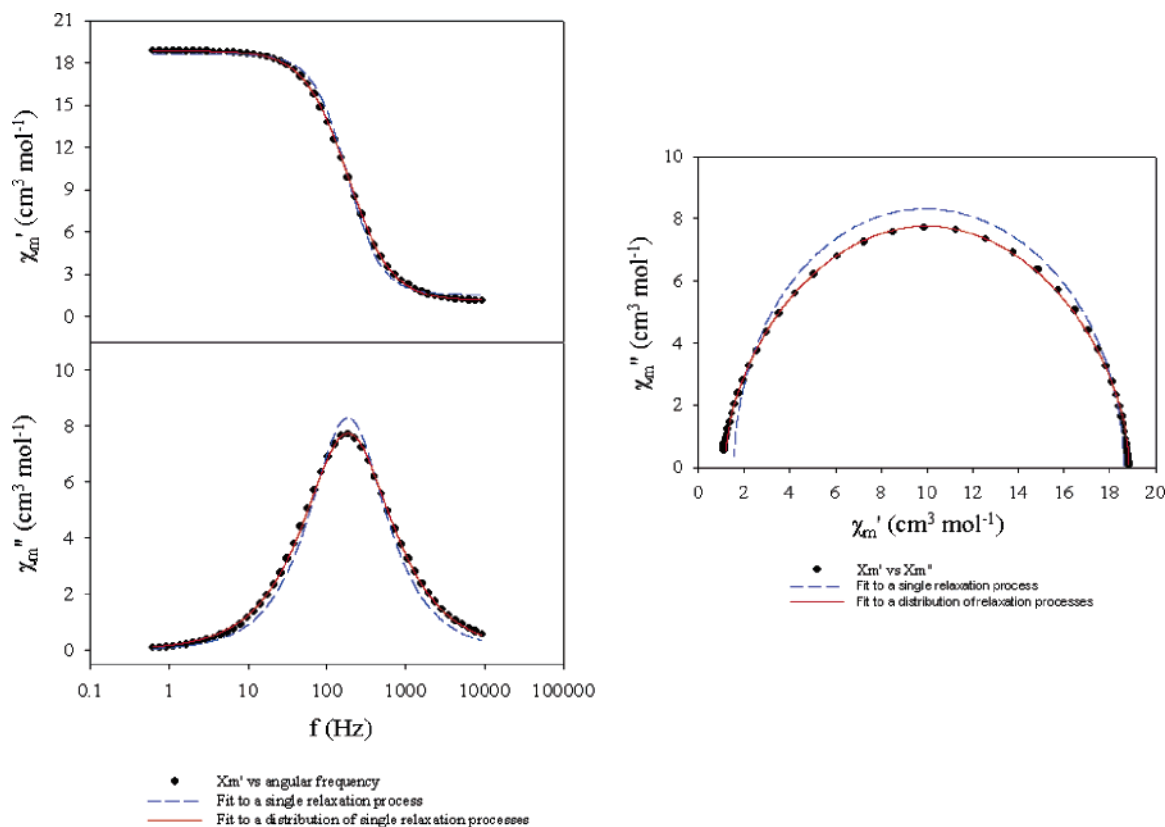
Figure 7. Plot of χ_M' versus frequency (top) and χ_M'' versus frequency (bottom) at 3.4 K for **3** (left). The dashed lines correspond to a fit to a single relaxation process, and the solid lines, to a fit to a distribution of single relaxation processes. Cole–Cole plot of χ_M' versus χ_M'' at 3.4 K for complex **3** (right). The dashed line corresponds to a fit to a single relaxation process, while the solid line is a fit to a distribution of single relaxation processes.

bonding interactions, the Mn(1) and Mn(3) become five-coordinate and square-pyramidal. Due to symmetry, the Mn-(1)Mn(2)Mn(3) and Mn(1′)Mn(2′)Mn(3′) planes are strictly parallel. O(1) is 0.09 Å out of the Mn(1)Mn(2)Mn(3) plane; the two oxide groups [O(1)] are directed toward the outside of the hexanuclear core. The three crystallographically independent Etsao^{2-} ligands adopt the $\eta^1:\eta^1:\eta^1:\mu$, $\eta^1:\eta^2:\eta^1:\mu_3$, and $\eta^2:\eta^1:\eta^1:\mu_3$ coordination modes (Scheme 2). In the crystal the molecules pack directly upon each other forming "2D-sheets", with each [Mn$_6$] complex then forming four intermolecular H-bonds to the solvate EtOH molecules, creating 1D "zigzag" chains between the sheets (Figure 3).

Complexes **2** and **3** are the first structurally characterized complexes of any metal that contain the dianionic form of EtsaoH$_2$, i.e., Etsao^{2-}, as ligand. The previously characterized complexes [Cu(EtsaoH)$_2$],[34a] [Ni(EtsaoH)$_2$],[34b] and [Pd-(EtsaoH)$_2$][34c] contain the ligand in its monoanionic form.

(34) (a) Lalia-Kantouri, M.; Uddin, M.; Hadjikostas, C. C.; Papanikolas, H.; Palios, G.; Anagnostis, S.; Anesti, V. *Z. Anorg. Allg. Chem.* **1997**, *623*, 1983. (b) Lalia-Kantouri, M.; Hartophylles, M.; Jannakoudakis, P. D.; Voutsas, G. P. *Z. Anorg. Allg. Chem.* **1995**, *621*, 645. (c) Voutsas, G. P.; Keramidas, K. G.; Lalia-Kantouri, M. *Polyhedron* **1996**, *15*, 147.
(35) (a) Xia, X.; Verelst, M.; Daran, J.-C.; Tuchagues, J.-P. *J. Chem. Soc., Chem. Commun* **1995**, 2155. (b) Kwak, B.; Rhee, H.; Park, S.; Lah, M. S. *Inorg. Chem.* **1998**, *37*, 3599. (c) Abbati, G. L.; Cornia, A.; Fabretti, A. C.; Caneschi, A.; Gatteschi, D. *Inorg. Chem.* **1998**, *37*, 1430. (d) Aromi, G.; Knapp, M. J.; Claude, J.-P.; Huffman, J. C.; Hendrickson, D. N.; Christou, G. *J. Am. Chem. Soc.* **1999**, *121*, 5489. (e) Kwak, B.; Rhee, H.; Lah, M. S. *Polyhedron* **2000**, *19*, 1985. (f) Brechin, E. K.; Coxall, R. A.; Parkin, A.; Parsons, S.; Tasker, P. A.; Winpenny, R. E. P. *Angew. Chem., Int. Ed.* **2001**, *40*, 2700. (g) Hoshino, N.; Ito, T.; Nihei, M.; Oshio, H. *Inorg. Chem. Commun.* **2003**, *6*, 377. (h) Li, B.; Han, D.-D.; Cheng, G.-Z.; Ji, Z.-P. *Inorg. Chem. Commun.* **2005**, *8*, 216. (i) John, R. R.; Lee, K.; Kim, B. J.; Suh, B. J.; Rhee, H.; Lah, M. S. *Inorg. Chem.* **2005**, *44*, 7109.

Complexes **1–3** join a rather small but growing family of Mn$^{III}_6$ complexes possessing the metal ions in various topologies.[11b,35] Three of them, namely [Mn$_6$O$_2$(OMe)$_6$(O$_2$CMe)$_2$L$^1_2$],[35a] [Mn$_6$O$_2$(OMe)$_6$(O$_2$CMe)$_2$L$^2_2$][35a] (L^1 and L^2 are trianionic Schiff bases), and [Mn$_6$O$_2$(O$_2$CH$_2$)$_{11}$(O$_2$CPe^t)(O$_2$CMe)(HO$_2$CPe^t)$_2$][11b] (Pe^{t}CO$_2$H = 2,2-dimethylbutyric acid) have cores based on two linked trinuclear [Mn$^{III}_3(\mu_3$-O)]$^{7+}$ units.

Magnetochemistry

DC Magnetic Susceptibility Studies: Direct current magnetic susceptibility studies were performed on polycrystalline samples of complexes **1–3** in the 5–300 K range in an applied field of 0.1 T. The results are plotted as the $\chi_M T$ product vs T in Figure 4. The $\chi_M T$ values at 300 K are 16.19, 18.99, and 19.23 cm^3 K mol^{-1} for **1–3**, respectively, close to the spin-only ($g = 2$) value of 18 cm^3 K mol^{-1} expected for a [Mn$_6$] unit comprising six high-spin Mn^{III} ions. For complex **1** the room temperature $\chi_M T$ value of 16.19 cm^3 K mol^{-1} decreases gradually as the temperature decreases until *ca.* 25 K when it then begins to increase to a maximum value of 10.39 cm^3 K mol^{-1} at 5 K. This behavior is consistent with the presence of both antiferromagnetic and ferromagnetic interactions between the metal centers with the low-temperature value indicating a relatively *small* ($S = 4$) spin ground state. Inspection of the molecular structure reveals the presence of (at least) three exchange pathways between the metal centers (Scheme 3): J_1 between Mn1 and Mn3 (and symmetry equivalent) mediated by the $-$N$-$O$-$ bridge of the oximate ligand (Mn1$-$N$-$O$-$Mn3 torsion angle, 18.0°), the bridging formate ligand, and the
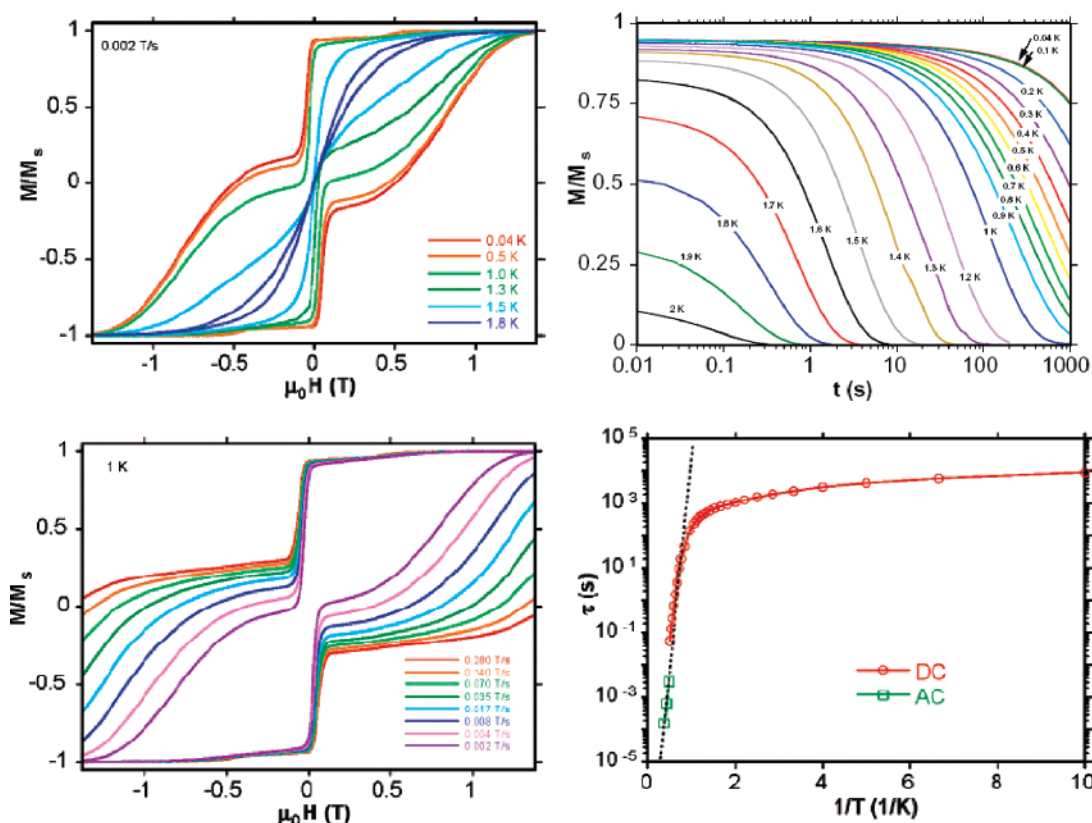
Figure 8. *M* vs *H* hysteresis loops for a single crystal of **1** (left). The loops are shown at different temperatures (top) and field sweep rates (bottom). *M* is normalized to its saturation value. Relaxation decay data (top right) plotted as M/M_S versus time. Arrhenius plot using powder ac and single-crystal dc data (bottom right); the dashed line is the fit of the thermally activated region.

oxide bridge; J_2 between Mn2 and Mn3 and between Mn2 and Mn1 (and s.e.) mediated only by the bridging $-N-O-$ moiety (Mn2$-$N22-O12$-$Mn3 torsion angle, 10.4°; Mn2$-$O11$-$N21$-$Mn1 torsion angle, 25.6°) and the oxide bridge; and J_3 between Mn1 and Mn1′ mediated by the monatomic oximato bridge (O13 and s.e.) and between Mn3 and Mn1′ (and s.e.) mediated by the diatomic oximato bridge (Mn3$-$N23$-$O23$-$Mn1′ and s.e.). Using the program MAGPACK and employing the spin Hamiltonian in eq 1 allowed us to satisfactorily simulate the data with the parameters $J_1 = -1.8$ cm^{-1}, $J_2 = -4.6$ cm^{-1}, $J_3 = +1.25$ cm^{-1}, and $g = 1.99$. This leads to a ground state of $S = 4$ with the first excited state ($S = 3$) located 8 cm^{-1} above the ground state.

$$\hat{H} = -2J_1(\hat{S}_1 \cdot \hat{S}_3 + \hat{S}_{1'} \cdot \hat{S}_{3'}) - 2J_2(\hat{S}_2 \cdot \hat{S}_3 + \hat{S}_2 \cdot \hat{S}_1 + \hat{S}_{2'} \cdot \hat{S}_{3'} + \hat{S}_{2'} \cdot \hat{S}_{1'}) - 2J_3(\hat{S}_1 \cdot \hat{S}_{1'} + \hat{S}_3 \cdot \hat{S}_{1'} + \hat{S}_{3'} \cdot \hat{S}_1) \quad (1)$$

For complex **2**, the room temperature $\chi_M T$ value of 18.99 cm^3 K mol^{-1} remains essentially constant as the temperature decreases until *ca.* 125 K when it then begins to increase to a maximum value of 27.79 cm^3 K mol^{-1} at 15 K, below which it decreases to 25.66 cm^3 K mol^{-1} at 5 K. This behavior is consistent with the presence of both antiferromagnetic and ferromagnetic interactions between the metal centers with the low-temperature value indicating an "*intermediate*" ($S = 7 \pm 1$) spin ground state. Even though inspection of the molecular structure reveals the presence of at least three exchange pathways between the metal centers, we were able to satisfactorily simulate the data assuming only a 2-*J* model: J_1 between the Mn1$-$Mn2, Mn1$-$Mn3, Mn1$-$Mn4, Mn3$-$Mn6, Mn3$-$
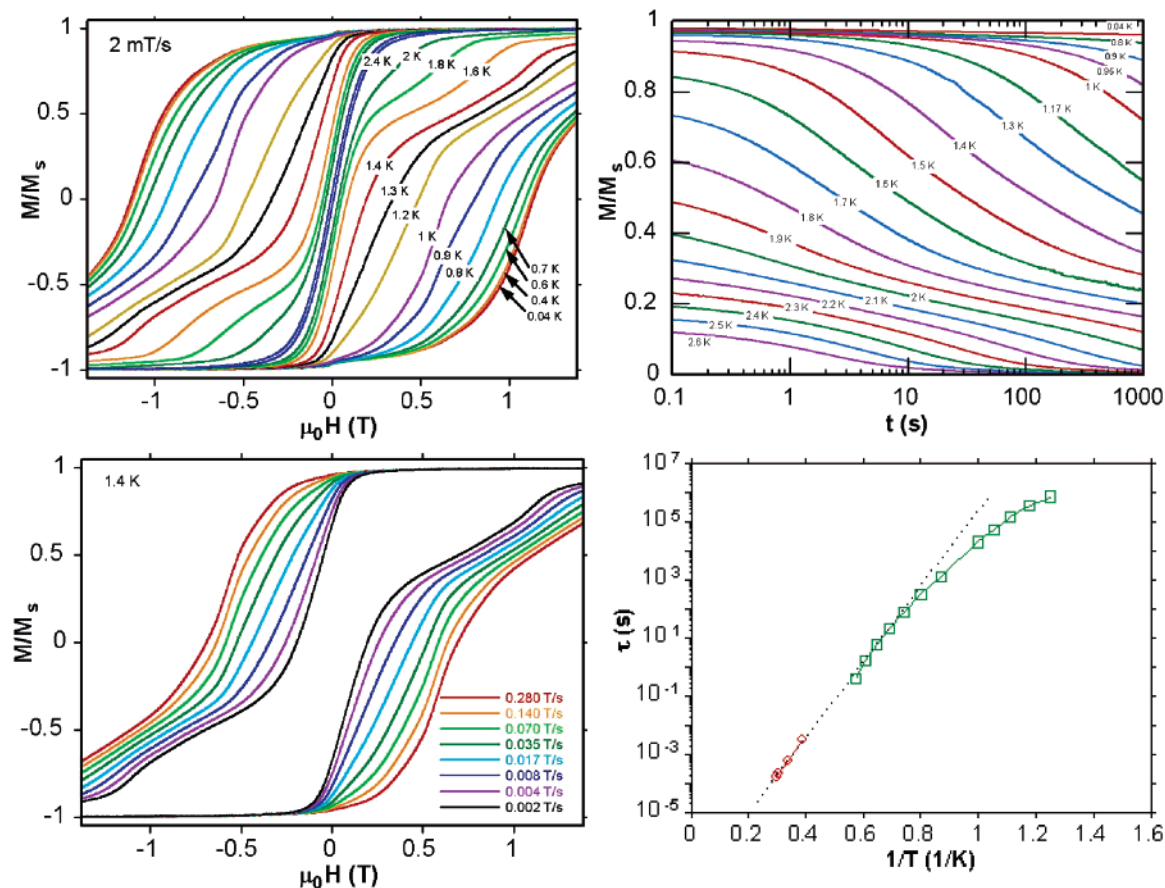
Mn4, Mn4$-$Mn6, and Mn4$-$Mn5 pairs; and J_2 between the Mn2$-$Mn3 and Mn5$-$Mn6 pairs (Scheme 4). Employing the spin Hamiltonian in eq 2 allowed us to satisfactorily simulate the data with the parameters $J_1 = +1.39$ cm^{-1}, $J_2 = -1.92$ cm^{-1}, and $g = 2.01$.

$$\hat{H} = -2J_1(\hat{S}_1 \cdot \hat{S}_2 + \hat{S}_1 \cdot \hat{S}_3 + \hat{S}_1 \cdot \hat{S}_4 + \hat{S}_3 \cdot \hat{S}_6 + \hat{S}_3 \cdot \hat{S}_4 + \hat{S}_6 \cdot \hat{S}_4 + \hat{S}_5 \cdot \hat{S}_4) - 2J_2(\hat{S}_3 \cdot \hat{S}_2 + \hat{S}_6 \cdot \hat{S}_5) \quad (2)$$

This suggests a ground state of $S = 7$, but with $S = 8$ and $S = 6$ excited states both located within 1 cm^{-1} of the ground state.

For complex **3**, the room temperature $\chi_M T$ value of 19.23 cm^3 K mol^{-1} increases slightly as the temperature decreases until *ca.* 125 K when it then begins to increase rapidly to a maximum value of 69.46 cm^3 K mol^{-1} at 5 K. This behavior is consistent with the presence of only ferromagnetic interactions between the metal centers with the low-temperature value indicating an $S = 12$ ground state. We were able to satisfactorily simulate the data by assuming a 1-*J* model (Scheme 5), despite the presence of (at least) two different interactions. Employment of a 2-*J* model neither enhanced the quality of the simulation nor changed the magnitude of exchange to any significant extent. Use of the Hamiltonian in eq 3 afforded $J = +0.93$ cm^{-1} and $g = 2.00$, with the $S = 11$ and $S = 10$ excited states 5 and 9 cm^{-1} above the $S = 12$ ground state, respectively.

$$\hat{H} = -2J(\hat{S}_1 \cdot \hat{S}_2 + \hat{S}_2 \cdot \hat{S}_3 + \hat{S}_1 \cdot \hat{S}_3 + \hat{S}_{1'} \cdot \hat{S}_{2'} + \hat{S}_{2'} \cdot \hat{S}_{3'} + \hat{S}_1 \cdot \hat{S}_{3'} + \hat{S}_3 \cdot \hat{S}_{1'} + \hat{S}_1 \cdot \hat{S}_{1'} + \hat{S}_1 \cdot \hat{S}_{3'}) \quad (3)$$

Figure 9. *M* vs *H* hysteresis loops for a single crystal of **2** (left). The loops are shown at different temperatures (top) and field sweep rates (bottom). *M* is normalized to its saturation value. Relaxation dc decay data (top right) plotted as M/M_S versus time. Arrhenius plot using powder ac (red circles) and single-crystal dc (green squares) data (bottom right); the dashed line is the fit of the thermally activated region.

In all three complexes the strength of the magnetic exchange is rather weak but appears to get more positive as the Mn–N–O–Mn torsion angle increases. In order to further determine the nature of the ground states of complexes **1**–**3**, variable temperature and variable field dc magnetization data were collected in the ranges 1.8–6 K and 0.5–7 T. In each case we attempted to fit the data using a matrix-diagonalization method to a model that assumes only the ground state is populated, includes axial zero-field splitting ($D\hat{S}_z^2$), and carries out a full powder average. The corresponding Hamiltonian is given by eq 4.

$$\hat{H} = D\hat{S}_z^2 + g\mu_B\mu_0 \, \hat{S}\cdot H \qquad (4)$$

where *D* is the axial anisotropy, μ_B is the Bohr magneton, μ_0 is the vacuum permeability, $\hat{S}_z$ is the easy-axis spin operator, and *H* is the applied field. The data for **1** and **3** are plotted as reduced magnetization ($M/N\mu_B$) versus *H/T* in Figure 5. For complex **1**, the best fit gave $S = 4$, $D = -1.39$ cm^{-1}, and $g = 1.99(3)$. Since both the dc and ac susceptibility data (vide infra) indicated the presence of low-lying excited states with smaller *S* values than the ground state, the magnetization data were fitted using only the high field (3–7 T) data. Including all fields (0.5–7 T) in the fits resulted in a poorer quality of fit, albeit with numbers of a similar magnitude. For complex **2** the best fit was for $S = 7$, $D = -0.75$ cm^{-1}, and $g = 1.99$, but this was (unsurprisingly) of rather poor quality. The presence of $S = 6$–8 states all within 1 cm^{-1} of each other means there is likely a significant

population of all three states even at low temperature, rendering the above numbers somewhat meaningless. This, in tandem with the maximum in $\chi_M T$ and the saturation of $M/N\mu_B$ at ∼14, implies a best "guess" of $S = 7 \pm 1$. This is further confirmed by the ac susceptibility (vide infra). For complex **3** the best fit, obtained using eight fields in the range 0.5–7 T, gave $S = 12$, $g = 1.99$, and $D = -0.43$ cm^{-1}.

Ac Magnetic Susceptibility Studies: Ac susceptibility measurements were performed on complexes **1**–**3** in 1.8–15 K in zero applied dc field and a 3.5 G ac field oscillating at 50–1500 Hz. For complex **1** the in-phase (χ_M', plotted as $\chi_M'T$ vs *T*, Figure 6) signal increases upon decreasing temperature, indicating the presence of low-lying excited states with smaller *S* values than the ground state. The signal displays a frequency-dependent decrease below ∼4 K, with a concomitant increase in the out-of-phase (χ_M'') signal. At a frequency of 1000 Hz the χ_M'' peak maximum occurs at approximately 3 K. A frequency dependent χ_M'' signal is a necessary (but in itself insufficient) piece of evidence indicating possible single-molecule magnetism behavior. The magnitude of the $\chi_M'T$ signal at 4 K supports the assignment of $S = 4$ for complex **1** in agreement with the dc data, and the magnitude of the χ_M'' signal suggests the slow relaxation to be real.

For complex **2** (Figure 6), the $\chi_M'T$ vs *T* signal decreases slightly upon decreasing temperature, suggesting the presence of excited states with larger *S* values than the ground state. Extrapolation of the signal above approximately 5 to 0 K gives a value of ∼27 cm^3 K mol^{-1} indicative of an $S = 7 \pm 1$ ground
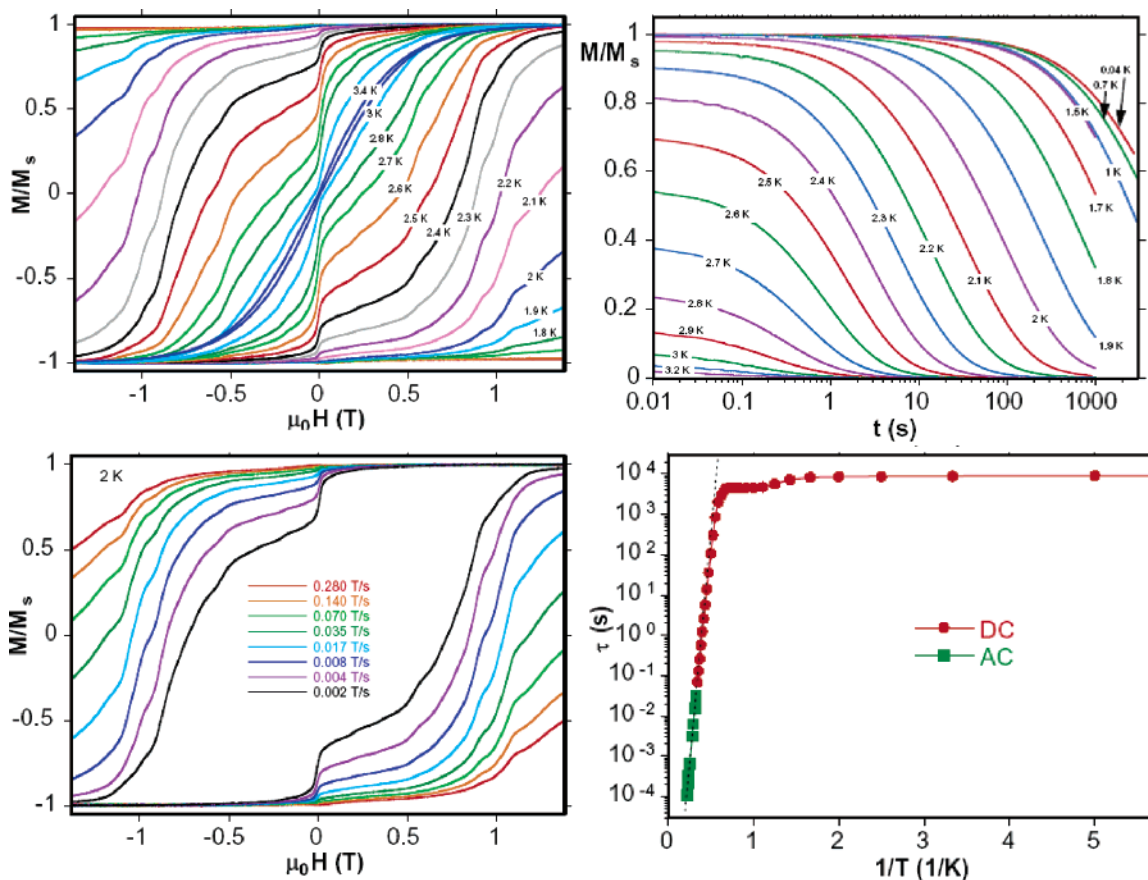
Figure 10. *M* vs *H* hysteresis loops for a single crystal of **3** (left). The loops are shown at different temperatures (top, sweep rate = 0.14 T/s) and field sweep rates (bottom, *T* = 2 K). *M* is normalized to its saturation value. Relaxation dc decay data (top right) plotted as *M*/*M*$_S$ versus time. Arrhenius plot using powder ac and single-crystal dc data (bottom right); the dashed line is the fit of the thermally activated region.

state, in excellent agreement with the dc data. Below approximately 5 K there is a frequency dependent decrease in the value of $\chi_M'T$ and a concomitant increase in the χ_M'' signal. Fully visible frequency-dependent out-of-phase, χ_M'', peaks are observed in a range of frequencies with the peak maximum at 1000 Hz occurring at approximately 3.75 K.

For complex **3** the value of the in-phase ($\chi_M'T$) signal increases with decreasing temperature to approximately 6 K, below which it displays a frequency-dependent decrease. This is indicative of the presence of excited states of smaller *S* values relatively close to the ground state. Extrapolation of the $\chi_M'T$ signal to 0 K from the small "plateau region" below 6 K gives a value of ~74 cm³ K mol⁻¹ indicative of an *S* = 12 ground state. Fully visible, frequency-dependent out-of-phase (χ_M'') ac susceptibility signals are seen below *ca.* 6 K with the peak at 1000 Hz occurring at approximately 4.5 K. The out-of-phase signals seen for all three complexes suggest **1–3** to be new SMMs and for **3** in particular to have a very large energy barrier for magnetization relaxation, with an upper limit of $U = S^2|D|$ = 89 K. In order to accurately determine these energy barriers, the ac χ_M'' data were used in combination with single-crystal dc decay measurements (vide infra).

For complex **3** ac susceptibility data were also measured as a function of the ac oscillation frequency at a constant temperature. In Figure 7 are shown plots of χ_M' versus frequency and χ_M'' versus frequency for a polycrystalline sample held at 3.4 K. The dashed lines result from the least-squares fitting of the data to a single relaxation process, to give $\chi_s = 1.56$ cm³

mol⁻¹, $\chi_T = 18.59$ cm³ mol⁻¹, and $\tau = 0.005\,54$ s (where χ_s is the adiabatic susceptibility; χ_T, the isothermal susceptibility; and τ, the magnetization relaxation time). Considerably improved fits (solid lines) are obtained when the data are fit to a distribution of single relaxation processes, with the parameters $\chi_s = 1.14$ cm³ mol⁻¹, $\chi_T = 18.84$ cm³ mol⁻¹, $\tau = 0.00544$ s, and $\alpha = 0.203$. The parameter α describes the width of the distribution. Figure 7 also shows a plot of χ_M' versus χ_M'' at 3.4 K. This type of plot (a Cole−Cole or Argand plot) is used to decide whether one or more relaxation processes are present: if symmetric, it is likely that only one process is present, as is the case for complex **3**, and again it is clear that fitting the data to a distribution of single relaxation processes (solid line) results in a better fit than fitting the data to a single relaxation process (dashed line).[36]

Single-Crystal Relaxation Studies and Hysteresis Loop Measurements: Dc magnetization decay data were collected on single crystals of **1–3** using a micro-SQUID apparatus and combined with the ac χ_M'' data. The combined data were then used to construct Arrhenius plots for all three complexes (Figures 8−10). The fits of the thermally activated regions gave the following: $\tau_0 = 2 \times 10^{-8}$ s and $U_{eff} = 28$ K for **1**; $\tau_0 = 3 \times 10^{-8}$ s and $U_{eff} = 30$ K for **2**; and $\tau_0 = 8 \times 10^{-10}$ s and $U_{eff} = 53.1$ K for **3**. The theoretical upper limits to the potential energy barriers to magnetization reorientation are $U = S^2 |D|$

---

(36) Aubin, S. M. J.; Sun, Z.; Pardi, L.; Krzystek, J.; Folting, K.; Brunel, L.-C.; Rheingold, A. L.; Christou, G.; Hendrickson, D. N. *Inorg. Chem.* **1999**, *38*, 5329.

≈ 22.2 cm^{-1} (31.8 K) for **1** and 61.9 cm^{-1} (88.7 K) for **3**. In each case U_{eff} is smaller than U, but for complex **3** this difference is of the order of 35 K, much larger than expected and much larger than that observed for other well-known SMMs. Possible explanations for this difference are given in the final discussion and conclusions section below. Hysteresis loops were observed for single crystals **1**–**3** whose coercivity was strongly temperature and sweep-rate dependent (Figures 8–10). For **1** hysteresis is observed up to approximately 1 K at a 2 mT/s sweep rate; for **2** hysteresis is observed up to approximately 2.4 K at a 2 mT/s sweep rate; and for **3** hysteresis is observed up to approximately 2.8 K at a 2 mT/s sweep rate. Each of the loops exhibit well-defined steps due to the rapid relaxation of the magnetization at a given magnetic field where a level crossing is avoided (quantum tunneling of magnetization, QTM). As the temperature is decreased, the number of molecules that undergo relaxation by thermal activation diminishes and those relaxing by tunneling increases. For **1** (Figure 8), at the indicated temperatures and $H = -1.4$ T all the molecules are in the $M_S = +4$ state of the $S = 4$ ground state. When the magnetic field is swept to zero, there is resonance between the $+4$ and the -4 M_S levels and part of the molecules tunnel to the $M_S = -4$ state, producing a step at $H = 0$. In this case, the height of the step indicates that the tunneling process is relatively fast.

For **2** the loops do not show the sharp steplike features associated with quantum tunneling of magnetization (QTM) and appear typical for a cluster with a distribution of energy barriers. The steps are present but broadened or smeared-out, due to an inherent disorder associated with either the molecule or the crystal and/or the presence of low-lying excited states. In this case the most likely source is Jahn–Teller isomerism since there appears little crystallographic disorder. Such disorder results in a distribution of Mn^{III} environments and hence a distribution in barrier heights. Such observations have been reported for many other (often large) SMMs.

The hysteresis loops for **3** are rather more complicated. The step positions arising from the ground state transitions are difficult to assign, and it is clear that the loops show many additional features (Figure 10). These additional steps probably originate from resonant tunneling between M$_S$ levels of the ground state, which are shifted to other fields due to fourth order anisotropy terms.[37] There might also be quantum resonances coming from tunneling between levels of the ground state and low-lying excited spin states. Indeed, susceptibility studies revealed the presence of low-lying excited states in very close proximity to the ground state, due to the weak exchange between the metal centers. The result is that, even at these temperatures, population of excited states, and hence excited-state tunneling, cannot be avoided. The presence of intermolecular interactions in the crystal and the "*lack*" of any molecular or crystallographic symmetry will also affect the loops, but these are likely to be of much less significance.

Final Discussion and Concluding Remarks

The two fundamental questions that need to be answered are (a) why the dominant magnetic exchange switches from antiferromagnetic to ferromagnetic in the complexes studied and (b) why the effective energy barrier for magnetization relaxation

for complex **3** is so heavily reduced (by $\sim$35 K) from its theoretical upper limit? In order to attempt to answer these questions we must first consider the "spin structure" for complex **1**. The $S = 4$ ground state results from the ferromagnetic interaction between two antiferromagnetically coupled ($S = 2$) Mn$^{III}_3$ triangles. The two different pairwise exchange interactions between the metals within each individual triangle are antiferromagnetic and weak; the exchange between triangles is ferromagnetic and weak. The oxide is 0.23 Å above the Mn$_3$ plane, and the Mn–N–O–Mn torsion angles are 25.6°, 18.0°, and 10.4°. In each complex the exchange *between* the two triangles remains weak and ferromagnetic. When moving to complex **2** the bridging within each triangle changes in two distinct ways: the carboxylate becomes terminal and the torsion angles of the oximate groups increase significantly to 36.9° (Mn1–Mn2), 42.1° (Mn3–Mn1), 23.3° (Mn2–Mn3), 32.4° (Mn5–Mn4), 42.2° (Mn4–Mn6), and 16.7° (Mn6–Mn5). The topology (but not the oxidation level) of the four central metals (Mn1, Mn3, and s.e.) now resembles that of the family of tetranuclear "planar diamond" complexes typified by [Mn$^{III}_2$-Mn$^{II}_2$(O$_2$CMe)$_2$(pdmH)$_6$]$^{2+}$ and its many subsequent analogues.[38] These molecules exhibit ferromagnetic exchange. The removal of the carboxylate bridge presumably removes an antiferromagnetic contribution to the exchange between Mn1 and Mn3 (and s.e.) and, in combination with an increase in the Mn3–N–O–Mn1 torsion angle ($\sim$42°), results in the ferromagnetic contribution dominating. The only aniferromagnetic exchange involves Mn2. It is connected to Mn1 and Mn3 via the central oxide and a Mn–N–O–Mn moiety, the former with a torsion angle of $\sim$37° and the latter with a torsion angle of $\sim$23°. The equivalent interaction in the upper triangle is between Mn5, Mn4, and Mn6 with torsion angles of 32.4° (Mn5–Mn4) and 16.7° (Mn5–Mn6). If we assume the larger torsion angles favor ferromagnetic exchange and smaller angles favor antiferromagnetic exchange, the result is competing exchange interactions and a Mn$^{III}_3$ triangle in which a degree of frustration exists, and hence a molecule with an intermediate ground state. On moving to complex **3** from **2**, the only major structural change is an increase in the Mn–N–O–Mn torsion angle for Mn5–Mn6 (and Mn2–Mn3) from $\sim$17° (and $\sim$23°) in **2** to $\sim$38° and 31° for Mn1–Mn2 and Mn2–Mn3, respectively in **3**. This results in all the exchange interactions being ferromagnetic and suggests that the increase in the Mn–N–O–Mn torsion angle (or the "twisting" of the oxime moiety) to be the origin of the ferromagnetism. The role of the central oxide in such triangular Mn topologies has always been the promotion of antiferromagnetic exchange between the metal centers. However, recently the triangular oxime-based complex [Mn$_3$O(mpko)$_3$(O$_2$CMe)$_3$] was shown to display ferromagnetic exchange.[17] Initial speculation as to why centered around the possibility of a decreasing magnitude of the AF contribution when the oxide became more nonplanar. However, the results here and elsewhere[39] suggest the origin to be the nonplanarity of the oxime linkage such that the ferromagnetic contribution it favors outweighs the AF contribution through the oxide.

Studies on single crystals of complex **3** reveal why the effective barrier is approximately 37 K below its upper limit. The magnitude of the magnetic exchange between the metal

(37) Wernsdorfer, W.; Murugesu, M.; Christou, G. *Phys. Rev. Lett.* **2006**, *96*, 057208.

(38) Brechin, E. K.; Huffman, J. C.; Christou, G.; Yoo, J.; Nakano, M.; Hendrickson, D. N. *Chem. Commun.* **1999**, 783.

(39) Milios, C. J.; Brechin, E. K. Unpublished results.

centers is weak, and the result is the presence of low-lying excited states. Hysteresis loop measurements at low temperatures reveal that tunneling occurs not only between the M_S states of the ground state but also between excited state M_S levels. In order to increase the value of U_{eff} toward U, and hence to record levels, the magnitude of J needs to be increased. We speculate that the way to do this is to further increase the Mn−N−O−Mn torsion angles, since the results presented here suggest that J becomes more ferromagnetic with increasing angle.

The 3-fold decrease in the magnitude of $|D|$ from **1** to **3** is also intriguing. We speculate the origin of this difference to be the change in coordination of two of the Mn ions from five-coordinate square-based pyramidal in **1** to six-coordinate distorted octahedral in **3**. This of course suggests that the isolation of $S = 12$ [Mn$_6$] analogues containing five-coordinate Mn ions may be a route to achieving SMMs with greatly enhanced energy barriers. Work to isolate such compounds is underway.

In conclusion, we can say that the deliberate structural distortion induced on a hexanuclear SMM by the introduction of bulkier carboxylates and oximes has switched the dominant magnetic exchange from antiferromagnetic to ferromagnetic, greatly enhancing the observed SMM properties. The origin of the ferromagnetic "switch" is based upon the following: (a) the exchange in the primary complex (**1**) is weak and this means that even small structural perturbations will be important in the relative magnitude and sign of J; (b) the dominant ferromagnetic contribution in the individual triangles can be induced by a combination of (i) the removal of competing antiferromagnetic exchange pathways (i.e., the carboxylate bridge) and (ii) an increase in the Mn−N−O−Mn torsion angles. At this stage it is difficult to speculate at which torsion angle the ferromagnetic contribution through the oxime moiety starts to outweigh the antiferromagnetic contribution through the oxide. This will require the synthesis of a family of related complexes. Initial (unpublished) results suggest this value may be around 31°.[39] Record values for U_{eff} can potentially be reached if analogues of complex **3** with increased "twisting" and hence increased J-values can be obtained.

Structural distortion has proven to be a valuable method for enhancing SMM properties and promises to produce a [Mn$_6$] analogue with a record anisotropy barrier; the method may be equally applicable to other SMM systems.

Supporting Information Available: Crystallographic details in cif format. This material is available free of charge via the Internet at http://pubs.acs.org.

JA070411G